Nat. Hazards Earth Syst. Sci., 8, 243–266, 2008
www.nat-hazards-earth-syst-sci.net/8/243/2008/

Natural Hazards and Earth System Sciences

The Papua New Guinea tsunami of 17 July 1998: anatomy of a catastrophic event

D. R. Tappin[1], **P. Watts**[2], **and S. T. Grilli**[3]

[1]British Geological Survey, Kingsley Dunham Centre, Keyworth, Nottingham, NG12 5GG, UK
[2]Applied Fluids Engineering, Inc., Private Mail Box #237, 6216 E. Pacific Coast Highway, Long Beach, CA 90803, USA
[3]Department of Ocean Engineering, University of Rhode Island, Narragansett, RI 02882, USA

Received: 30 August 2005 – Revised: 24 May 2007 – Accepted: 21 February 2008 – Published: 26 March 2008

Abstract. The Papua New Guinea (PNG) tsunami of July 1998 was a seminal event because it demonstrated that relatively small and relatively deepwater Submarine Mass Failures (SMFs) can cause devastating local tsunamis that strike without warning. There is a comprehensive data set that proves this event was caused by a submarine slump. Yet, the source of the tsunami has remained controversial. This controversy is attributed to several causes. Before the PNG event, it was questionable as to whether SMFs could cause devastating tsunamis. As a result, only limited modelling of SMFs as tsunami sources had been undertaken, and these excluded slumps. The results of these models were that SMFs in general were not considered to be a potential source of catastrophic tsunamis. To effectively model a SMF requires fairly detailed geological data, and these too had been lacking. In addition, qualitative data, such as evidence from survivors, tended to be disregarded in assessing alternative tsunami sources. The use of marine geological data to identify areas of recent submarine failure was not widely applied.

The disastrous loss of life caused by the PNG tsunami resulted in a major investigation into the area offshore of the devastated coastline, with five marine expeditions taking place. This was the first time that a focussed, large-scale, international programme of marine surveying had taken place so soon after a major tsunami. It was also the first time that such a comprehensive data set became the basis for tsunami simulations. The use of marine mapping subsequently led to a larger involvement of marine geologists in the study of tsunamis, expanding the knowledge base of those studying the threat from SMF hazards. This paper provides an overview of the PNG tsunami and its impact on tsunami science. It presents revised interpretations of the slump architecture based on new seabed relief images and, using these, the most comprehensive tsunami simulation of the PNG event to date. Simulation results explain the measured runups to a high degree. The PNG tsunami has made a major impact on tsunami science. It is one of the most studied SMF tsunamis, yet it remains the only one known of its type: a slump.

Correspondence to: D. R. Tappin
(drta@bgs.ac.uk)

1 Introduction

When the Papua New Guinea (PNG) tsunami struck on the evening of 17 July 1998, devastating three villages with the loss of over 2200 lives, the potential hazard from tsunamis caused by Submarine Mass Failures (SMFs) was recognised, but not fully grasped (e.g. Ward, 2001; Bardet et al., 2003). There was limited appreciation that the magnitude of tsunamis generated by SMFs was dependent upon the mode of failure. SMFs include all forms of seabed sediment movement that may be regarded by their end members as ranging from translational sediment flows with long runouts, formed most often by sands and silts and soft mud, to rotational slumps which, by comparison to sediment flows, have restricted horizontal movement and are formed mainly in cohesive mud. Thus before 1998, although there had been previous research on SMFs, this work was not generally in the context of their potential to generate destructive tsunamis which would have a major coastal impact. The PNG tsunami changed this perspective. It illustrated that SMFs can cause devastating local tsunamis. It led to a fundamental reappraisal of the hazard from SMFs. It also illustrated that the specific mechanism of SMF (rotation or translation) is a major control on tsunami magnitude (Grilli and Watts, 2005; Watts et al., 2005a).

Published by Copernicus Publications on behalf of the European Geosciences Union.

Although the PNG event has had a major impact on tsunami science, the cause of the local tsunami has remained controversial (e.g. Geist, 2000; Imamura et al., 2003; Satake et al., 2003). This controversy continues despite the comprehensive data set acquired while researching the disaster, and the large number of publications addressing the event. Over 40 scientific papers have been published on the tsunami (e.g. Synolakis et al., 2002; Tappin et al., 1999, 2001, 2002, 2003). The event was the subject of special workshops, as well as numerous sessions at international scientific meetings (e.g. Hebenstreit, 2001; Bardet et al., 2003; Tappin, 2004). The far field tsunami was probably caused by the earthquake, but for many scientists an earthquake source for the local tsunami is still considered a likely alternative or, at the very least, a contributory factor (e.g. Geist, 2000; Satake et al., 2003).

The purpose of this paper is therefore threefold. 1) To present new interpretations of multibeam bathymetric and seismic data from which we readily identify a slump feature offshore of northern PNG. 2) That new modelling based on these interpretations proves the 1998 PNG tsunami in the near field was caused by an underwater sediment slump, probably triggered by an earthquake, and not by the earthquake itself. Models based on the slump source recreate the tsunami wave to an acceptable degree of precision. 3) Finally, to gain a better understanding of why the tsunami was such a seminal event and why its source has remained controversial.

2 Background

The potential for SMFs to generate tsunamis has been known for over 100 years (Milne, 1898; de Ballore, 1907; Gutenberg, 1939). Of the more recent SMF events, most have involved some degree of controversy, at least initially. One example is the Grand Banks event of 1929 (Heezen and Ewing, 1952; Heezen et al., 1954; Terzaghi, 1956; Piper and McCall, 2003). Other tsunamis that may involve SMFs such as Unimak, Alaska, 1946, and Sanriku, 1896, were considered primarily in the context of their earthquake source (e.g. Abe, 1979; Johnson and Satake, 1997). It is only recently that a SMF was shown to be a likely cause of the 1946 Alaska event, almost certainly locally and possibly in the far-field as well (Fryer et al., 2004; López and Okal, 2006; Waythomas et al., 2008[1]). The Flores Island tsunami of 1992 has been largely neglected, even though it is likely that, as with Alaska, 1946, both earthquake and landslide sources contributed to the event (Imamura and Gica, 1996; Imamura et al., 1995).

Previous to the PNG tsunami, simulations of tsunami generation were mainly confined to earthquake sources (e.g. Hammack, 1973). Earthquake sources were based on the assumption that the initial water surface deformation was instantaneous and equal to that at the seabed. Seabed deformation was calculated from earthquake fault parameters (e.g. Okada, 1985). Underwater landslides were considered to be ineffective at generating significant tsunamis because of their longer source generation times, smaller areas of seabed disturbance, and the directivity of the tsunami produced (Hammack, 1973; LeBlond and Jones, 1995). Modelling of SMFs was mainly confined to translational events (e.g. Jiang and LeBlond, 1992, 1994) such as those defined by Hampton (1972). A complication in understanding tsunamis generated by SMFs is the variety of their failure mechanisms, which may be classified according to morphology, sediment type, or kinematics (see Hampton et al., 1996; Turner and Schuster, 1996; Keating and McGuire, 2000; O'Grady et al., 2000). The type of SMF is determined mainly by its sediment composition, which controls SMF morphology and kinematics. Tsunami generation models were based on depth-averaged wave equations that represented immiscible liquids, or water with a Bingham plastic (e.g. Jiang and LeBlond, 1992, 1994). Whereas depth averaging accurately applies to tsunami generation from earthquakes, it is questionable when applied to landslide tsunamis, because it does not allow for vertical fluid accelerations, which are important during SMF motion and tsunami generation (Grilli et al., 2002). In 1998, the landslide constitutive equations used in modelling were largely untested by laboratory experiments or case studies. SMF models were not based on geological data, but idealised SMF morphologies. There was no established method of merging geological data with SMF models. In total, there was little appreciation of the complexity of modelling tsunamis generated by different SMF mechanisms.

3 The Papua New Guinea tsunami of 1998

The basic facts relating to the PNG event are well established. An earthquake of magnitude 7.1 struck the northern coast at 08:49 GMT (18:49 local time) on 17 July 1998 (Fig. 1; Davies, 1998; Kawata et al., 1999). The earthquake magnitude was small in comparison to the 10–15 m high tsunami that devastated the coast around Sissano Lagoon. There was no evidence to suggest that the earthquake was a "tsunami earthquake" (Kanimori, 1972) and, based on Newman and Okal's (1998b) discriminant of E/M_0, the earthquake did not possess "slow" source characteristics. (These authors define "slowness" using the ratio between high-frequency energy E and low-frequency seismic moment M_0. Compared to an average value of -4.98, the main shock was computed at -5.67, indicating a moderate deficiency in E, and the aftershock at -4.72, a normal rupture speed, neither of which indicates a tsunami earthquake.) Simulations of the tsunami based on a shallow dipping thrust (the most probable earthquake failure mechanism) did not

[1] Waythomas, C. F., Watts, P., Shi, F., and Kirby, J. T.: Pacific basin tsunami hazards associated with mass flows in the Aleutian Arc of Alaska, Quat. Sci. Rev., in review, 2008.

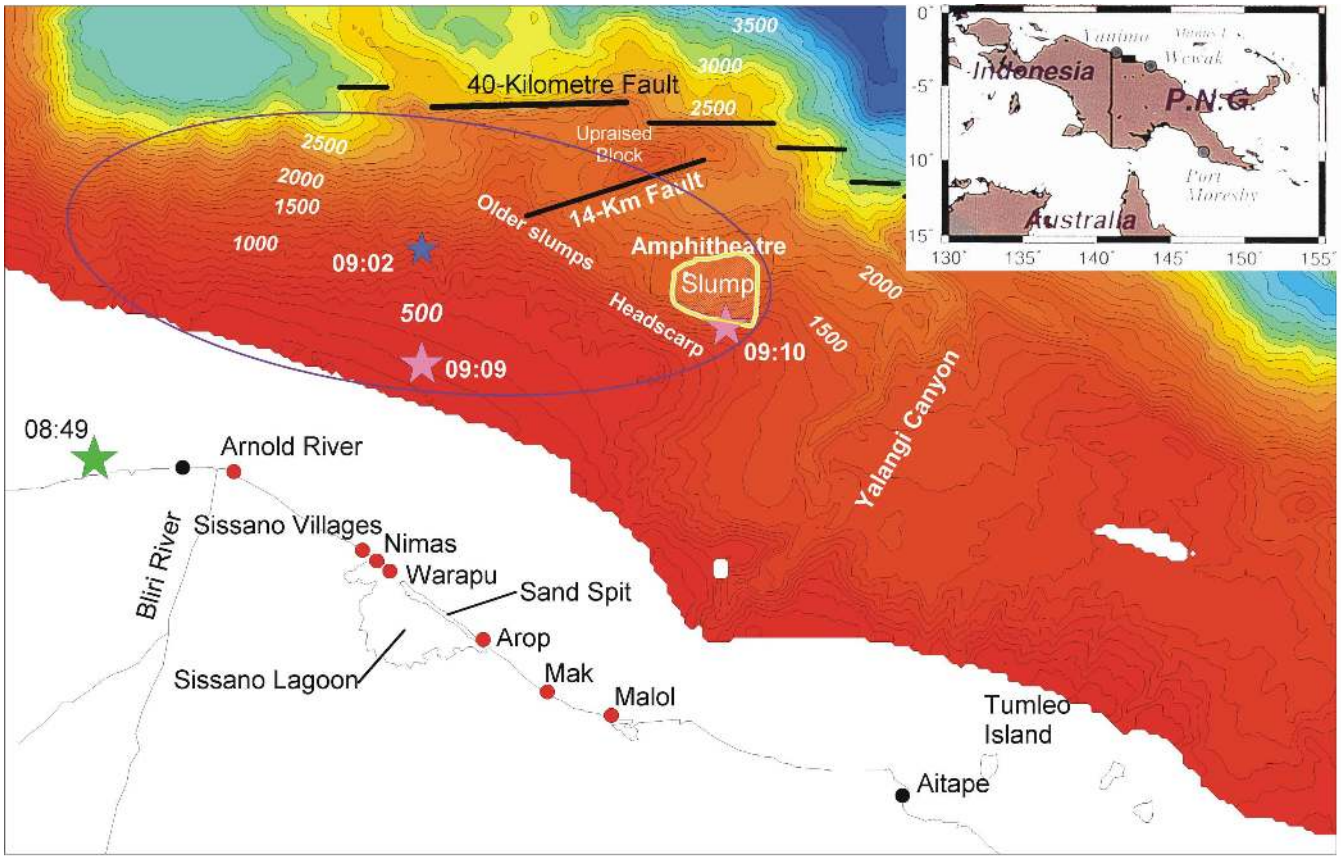

Fig. 1. Location map of the northern PNG coast struck by the tsunami of July, 1998 and bathymetry from the 1999 *Kairei* survey. Also shown is the earthquake epicentre (Green star), the aftershocks of 09:09:30 and 09:10:00 (pink stars), the T-phase slump signal of 09:02 (blue star – with error ellipse in blue from Synolakis et al., 2002), the main villages destroyed (red dots), the slump area, and main seabed features. Water depths are in metres.

approach the runup measured during the onshore field surveys, or match the wave arrival times from eyewitness accounts (e.g. Titov and Gonzalez, 1998; Davies, 1998; Kawata et al., 1999; Matsuyama et al., 1999). The location of the earthquake epicentre just offshore and to the northwest of Sissano would have resulted in an almost immediate wave impact, not corresponding to the ∼20 min delay reported by survivors. The peaked runup distribution along the coast did not indicate a presumably broad earthquake source. From the outset it was likely that a tsunami source other than an earthquake was involved, the most likely alternative being a SMF (e.g. Newman and Okal, 1998a, b; Titov and Gonzalez, 1998; Geist, 1998a; Takahashi and Kawata, 1998).

Without data from offshore, there would have been no opportunity to confirm or refute the suggestion that a SMF may have caused or contributed to the tsunami. However, in early 1999, the Japanese government funded, through the Japan Marine Science and Technology Center (JAMSTEC) two marine surveys to investigate the seabed off the north coast of PNG. The objective was to discover whether there was a SMF offshore of Sissano Lagoon and, if so, whether it could have generated the tsunami. The first two surveys were followed in September of the same year by a survey led by the University of California at Santa Cruz (UCSC). In 2000 and 2001, there were two additional surveys funded by Japan and again sponsored by JAMSTEC and SOPAC. The first published results of the offshore surveys and preliminary modelling concluded that an offshore slump was the most likely source of the local tsunami (Tappin et al., 1999), an interpretation confirmed by subsequent marine geology research (Tappin et al., 2001, 2002, 2003; Sweet and Silver, 1999, 2003).

Notwithstanding the initial results of the offshore surveys, the debate over the source of the tsunami continued (e.g. Matsuyama et al., 1999; Satake and Tanioka, 1999; Tanioka, 1999; Geist, 2000). Far-field earthquake evidence was used to justify a steeply-dipping thrust as the rupture mechanism (Kikuchi et al., 1999), despite the fact that this was unlikely because the aftershock distribution indicated a shallow dipping rupture (McCue, 1998). In addition, the marine surveys showed that almost all major faults offshore were dip-slip (Tappin et al., 1999). Simulations based on a tsunami source

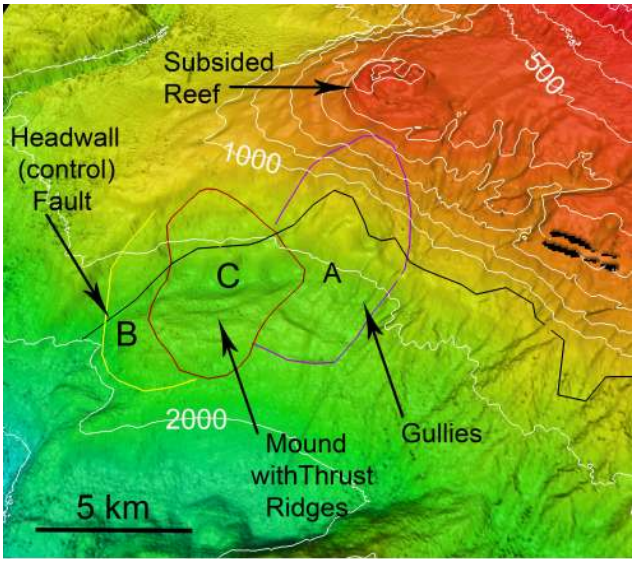

Fig. 2. 3-D image of the Amphitheatre viewed from the northwest. The three slumps (A, B and C, labelled by decreasing age) are identified together with the control fault at the base of the headscarp. Note the change in seabed morphology from the heavily gullied area in the right of the image (slump A) to that to the left (slumps B and C), where gullies are absent. Water depths are in metres. Vertical exaggeration 3×. See text for discussion.

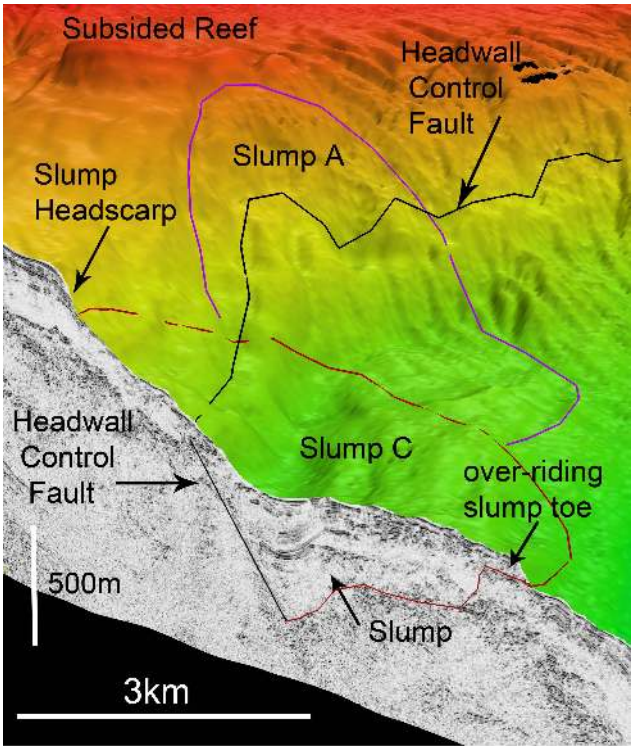

Fig. 3. 3-D image of the Amphitheatre, including seismic cutaway of slump C, viewed from the northeast. The headwall of the slump coincides with a control fault. This fault channelled artesian water pumped up from depth to the slump failure surface, triggering the slump itself around 12 min after the main shock. Vertical exaggeration 3×. See text for discussion.

from translational landslides (e.g. Hampton, 1972) could not reproduce the measured runup (see papers presented at the IUGG meeting in July, 1999 and published in Hebenstreit, 2001). Although the first published results of the marine surveys identified a slump as the likely source (Tappin et al., 1999), translational landslide sources were still considered to be the most likely mechanism of failure and tsunami generation (e.g. Matsuyama et al., 1999; Geist, 2000). With no local tide gauge data, the reports from survivors on the 20 min time lag between the earthquake and tsunami were discounted (e.g. Geist, 2000). Despite the additional evidence from the marine surveys of late 1999 (Sweet and Silver, 1999) and early 2000 (Tappin et al., 2001), together with the preliminary numerical simulations (Watts et al., 1999) that confirmed an offshore sediment slump as the most likely tsunami source, arguments on the source mechanism continued (Geist, 2001; Imamura and Hashi, 2003; Okal and Synolakis, 2001; Satake and Tanioka, 2003; Tappin et al., 2001; Synolakis et al., 2002; papers in Bardet et al., 2003).

4 Marine geology

During the marine surveys, a comprehensive geophysical data set was acquired off northern PNG, with over 19 000 km^2 of multibeam bathymetry, 4.2 kHz high-resolution sub-bottom seismic lines (SBSL), and both single (SCS) and multichannel seismic (MCS) data. In the region of the slump, four 7 m long sediment piston cores were recovered together with numerous shallow (30 cm) push cores of sediment, rock samples, and marine organisms. Still and video photography of the seabed were acquired by a tethered Remotely Operated Vehicle (ROV) and Manned Submersible (MS). This data set has been fully reported on (Tappin et al., 1999, 2001, 2002, 2003; Sweet and Silver, 2003). It has contributed to PNG tsunami analysis by providing a comprehensive understanding of: (i) the background tectonics and sedimentation regime of the area; (ii) the slump and its architecture; and (iii) the relative timing of slump failure. Here, we focus on the area termed the 'Amphitheatre', in which lies the slump, considered as the most likely source of the 1998 tsunami (Fig. 1). Our new interpretations are based on visualisations of seabed relief integrated with seismic reflection profiles using *Fledermaus*, an interactive visualisation software (Figs. 2 and 3).

The arcuate shape of the Amphitheatre indicates a likely formation by submarine slope failure along a control fault located along the base of the headscarp (Figs. 1, 2 and 3). Integration and reinterpretation of the multibeam bathymetry with the SCS and MCS, using *Fledermaus*, has resulted in improved interpretations of slumping within the

Amphitheatre (Figs. 2 and 3). The new interpretation shows that there are three phases of slumping. There are two older slumps (A and B) located in the east and west of the Amphitheatre, that are both cut by the youngest slump (C) that lies in the centre and is interpreted as failing on 17 July 1998. The western slump (A) is identified by its heavily gullied surface with arcuate thrust ridges and a headscarp traced upward to the foot of the subsided reef (Fig. 2). The eastern slump (B), (described by Sweet and Silver, 2003) is probably younger than slump A in the west, as its surface is not as heavily gullied. Both A and B are truncated by slump C. On the surface of slump C, on the elevated mound below the headscarp, there are curvilinear, but generally east-west trending ridges and furrows, that are convex towards the north and clearly terminate at the eastern and western boundaries of the slump. These features are the surface expression of small thrust faults (or pressure ridges) that are imaged on the seismic data and which formed during downslope movement of the slump. On the seismic surveys, the slump toe overrides the underlying strata, a relationship typical of slumping in cohesive sediments (Fig. 3). The youngest slump terminates the thrust ridges of older slumps A and B to both the east and west. The data confirms previous interpretations that there is downslope sediment movement in the Amphitheatre and that this movement is of limited horizontal extent. There is no further sediment runout below the mound that would indicate a translational failure, such as landslide or sediment flow. The new interpretation also confirms that the failures in the Amphitheatre are slumps. The youngest central slump has a width of ∼4.2 km, a length of ∼4.5 km, and a thickness of ∼750 m. The slump volume is estimated to be around 6.4 km^3.

5 Tsunami modelling

Modelling of the PNG tsunami source based on a slump in the Amphitheatre took place in three phases. Preliminary modelling took place onboard the *Kairei* in January 1999 as the first data were acquired (published in Tappin et al., 1999). A subsequent phase of modelling took place after the first two marine surveys (Tappin et al., 2001; Watts et al., 2003). More recent modelling has been undertaken over the past three years. The results of these phases are shown in Fig. 4a–c.

Our most recent modelling results (Fig. 4d) are based on the revised slump architecture presented above. The new modelling also benefits from recent advances made in understanding tsunami generation from SMFs, that have now clarified and/or validated assumptions made previously (Grilli et al., 2005; Watts et al., 2005a; Enet and Grilli, 2007). We have also refined the grid spacing, and in place of the previous 100×100 m grid we have now used a uniform 50×50 m grid. For the tsunami propagation and inundation model (see Watts et al., 2003), we use FUNWAVE, a fully nonlinear and dispersive (so-called "Boussinesq") long wave model that simulates the more dispersive SMF tsunamis far better than traditional nonlinear shallow water (NSW) wave models. FUNWAVE also includes well-calibrated dissipation models for wave breaking and bottom friction (Wei and Kirby, 1995; Wei et al. 1995; Chen et al., 2000; Kennedy et al., 2000). Finally, we now use the actual time of slump failure (to within approximately 45 s) as identified by the m_b=4.4 aftershock at 09.02 (GMT), as well as T-phase records made at the same time (Okal et al., 1999; Synolakis et al., 2002). (There is a 45-s error bar in the timing of the T-Phase because of uncertainty between the relationship of the T-Phase signals and the roughly 100-s duration of slump failure. To account for these uncertainties, we have assumed that the two kinds of signals correlate with the middle period of slump movement, when seismic waves and T-phase sounds would presumably be strongest.)

With regard to tsunami generation, based on the revised dimensions for slump C, we calculate a basal shear strength of $S_u \approx 0.8$ MPa, with a corresponding Coulomb friction coefficient of $C_n \approx 0.11$. Using the equations of motion detailed in Grilli and Watts (2005), which are similar to those of Watts et al. (1999), we calculate a characteristic time of slump motion, t_o=32 s, an initial acceleration a_o=0.47 m/s^2, and a maximum velocity $u_{\max}$=15 m/s, occurring approximately 50 s after slump failure. The slump comes to rest after ∼100 s, at which time its centre of mass has advanced ∼980 m downslope towards an azimuth of 349°. The initial water depth over the middle of the slump is 1420 m. These results are the tsunami source parameters. In our simulations, the transformation of a 2-D into a 3-D tsunami source uses mass conservation considerations along the third dimension (Watts et al. 2005a; Grilli et al., 2002; Enet et al., 2005, 2007). In the most recent simulations, both the free surface shape and horizontal velocities of the 3-D slump tsunami source calculated at time $t=t_o$ are specified as initial conditions in FUNWAVE.

Unlike NSW model results (Fig. 4a, b), FUNWAVE produces onland runups (Fig. 4c, d), not offshore maximum wave heights, as previously modelled by various research groups (e.g. Tappin et al., 2001; Synolakis et al., 2002). Peak runup is located on the sand spit in front of Sissano Lagoon and is directly comparable to onland measurements made during field surveys. Time series snapshots of the tsunami approaching Sissano Lagoon are shown in Fig. 5. These snapshots are based on a 100×100 m grid and are for demonstrative purposes, because offshore propagation and times of arrival are similar to those modelled on the 50×50 m grid. Figure 5a shows the sequence of waves travelling away from the slump source, 15.6 min after the main shock and 3.1 min into tsunami propagation. In the direction of the open ocean, there is a leading elevation wave (barely shown), followed by two pairs of depression and elevation waves. In the landward direction, there is a leading depression wave followed by two pairs of elevation and depression waves. In deep

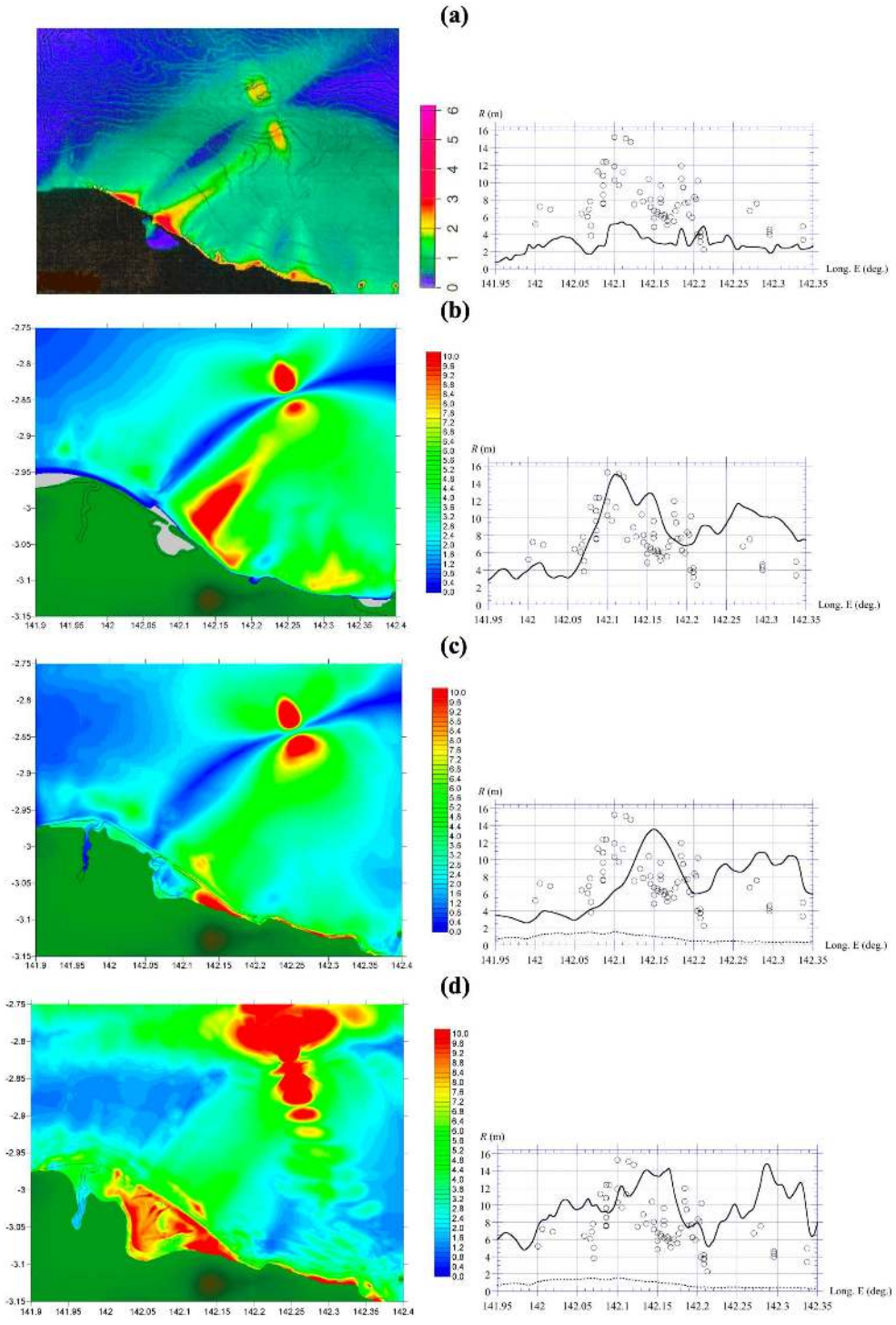

Fig. 4. Evolution of slump generated tsunami simulations and runup over the last several years: **(a)** an improvised landslide tsunami source combined with linear shallow water wave results from the *Kairei* cruise (maximum wave heights are taken from the 10 m water depth contour), **(b)** a landslide tsunami source from TOPICS 1.1 combined with nonlinear shallow water wave results from TUNAMI-N2 (maximum wave heights occur several kilometres offshore), **(c)** a landslide tsunami source from TOPICS 1.2 combined with the fully nonlinear and dispersive model FUNWAVE (maximum runup occurs onshore), and **(d)** a revised FUNWAVE simulation based on the new slump architecture given herein [maximum runup occurs onshore] and a uniform 50×50 m grid spacing. Solid line – modelled, circles – measured runup, dotted line in (c) and (d) – co-seismic tsunami simulation.

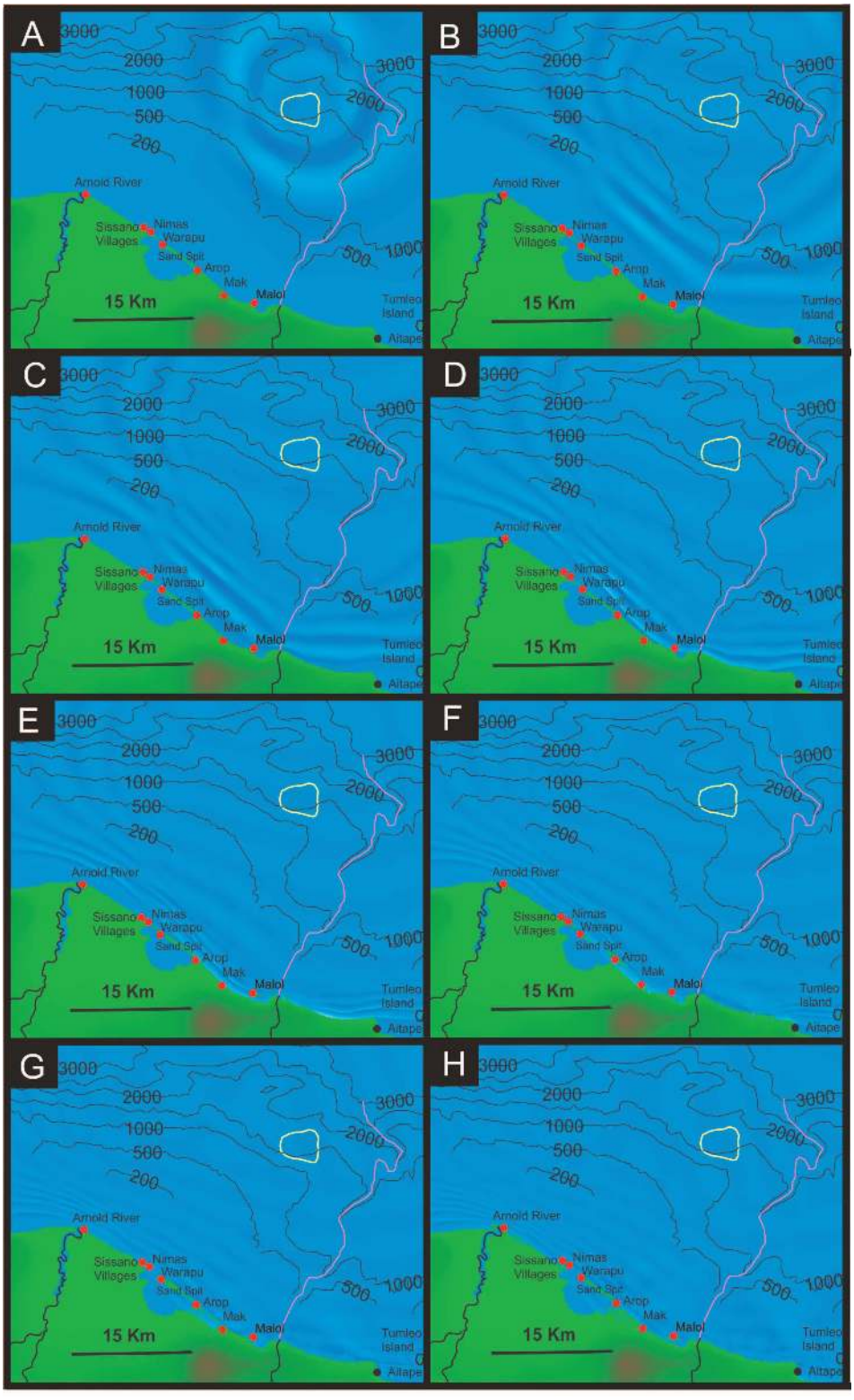

Fig. 5. Eight snapshots of tsunami propagation and inundation using FUNWAVE, a uniform 100×100 m grid spacing, and the latest slump source. Light blue are elevation waves and dark blue are depression waves. (Time after main shock; time after slump initiation). **(a)** [15.6 min; 3.1 min]. **(b)** [18.6 min; 6.1 min]. **(c)** [20.1 min; 7.6 min]. **(d)** [21.6 min; 9.1 min]. **(e)** [23.2 min; 10.7 min]. **(f)** [24.7 min; 12.2 min]. **(g)** [26.2 min; 13.7 min]. **(h)** [27.7 min; 15.2 min]. The slump location is in yellow, and Yalingi Canyon is marked in purple. See text for further discussion.

water, this pattern is symmetric and oriented in the direction of mass failure. 18.6 min after the earthquake (Fig. 5b), there are three clearly imaged elevation waves travelling towards Sissano Lagoon. Frequency dispersion has transferred energy from the first two elevation waves into the third one as it propagates towards shore. 20.1 min after the earthquake (Fig. 5c), the first elevation wave is about to strike the village of Malol. The deep-water Yalingi Canyon off Malol, together with the small bay to the west of the village, focuses the water waves away from the village. In the deep water off Malol, the waves propagate faster than elsewhere, explaining the fact that Malol is struck first by the tsunami. Farther northwest, the first elevation wave is breaking roughly 3 km off Sissano Lagoon.

After 21.6 min (Fig. 5d), the first elevation wave has already broken off Sissano Lagoon and is propagating towards the beach as a bore. The second elevation wave is about to break or is breaking further offshore. The wave breaking is localized off Sissano Lagoon because the shallow shelf has acted as a lens, focusing wave energy towards the sand spit. The tsunami has inundated most of Malol and is about to arrive at Aitape, near the eastern edge of the image. 23.2 min after the earthquake (Fig. 5e), the first wave attacks the shore near the village of Arop, with devastating consequences, and the second wave is close behind, propagating as a bore towards the sand spit. Malol has been completely inundated whereas, further east, Aitape is just about to undergo tsunami attack. After 24.7 min (Fig. 5f), the first elevation wave is sweeping obliquely across the last part of the sand spit and is beginning to inundate Sissano village, located on the west side of the lagoon entrance. Near Malol, tsunami attack is nearing its maximum inland inundation. At Aitape, the tsunami attack is under way within the village. After 26.2 min (Fig. 5g), the second elevation wave passes over the sand spit, near where the village of Arop once stood. The first elevation wave is traversing Sissano Lagoon. Sissano village has been completely inundated in the west, while Aitape has been completely inundated in the east. Finally, 27.7 min after the earthquake and 15.2 min after the slump failed (Fig. 5h), the first elevation wave continues to traverse the lagoon. The third elevation wave is just arriving at the sand spit. Elsewhere, in the most devastated areas, water is receding back to the sea. Smaller water waves continue to attack other shorelines, but with less consequence than for the area around Sissano Lagoon.

6 Discussion

6.1 New geological interpretations of PNG

Our new interpretation of the Amphitheatre area off Sissano Lagoon shows that three slumps are present, whereas previously we identified only one (Tappin et al., 1999, 2001, 2002, 2003). The youngest slump C (Figs. 2 and 3) is located in the centre of the Amphitheatre. Its young age is evidenced by the seabed morphology that illustrates its relationship to the older slumps on either side. The corrugated surface morphology (caused by the thrusts within the slump) of the basal mound on slump C contrasts with the deeply incised (gullied) seabed in the western part of the Amphitheatre where slump A is located. The eastern margin of slump C is delineated by the termination of the thrust folds, and the slightly elevated surface of the basal mound. To the east of this margin we identify a backward rotated failure from the MCS of Sweet and Silver (2003). The contrasting seabed morphology within the Amphitheatre, together with the slumps identified on the seismic data, confirms that there are three slumps present. The youngest slump is restricted to a discrete area, indicating a rotational cohesive failure. There is no evidence to indicate the presence of a translational landslide.

Confirmation that the central slump is the youngest of the three failures is from seabed photographs and video images (Tappin et al., 2001). These images show that the main concentration of seabed disturbance is in the central part of the Amphitheatre where slump C is located. The main area of deformation is located where the slump control fault intersects the seabed (Figs. 2 and 3). This visual evidence includes recently exposed sediment fissures with sharply defined edges located on the mound, and along the slump headscarp where we observe angular cohesive sediment blocks. Along the seabed expression of the control fault there is active fluid venting, with an associated chemosynthetic biota of mussels and tube worms that increase in density towards the central area of the slump at the foot of the steep scarp slope. There are numerous black mounds on the seabed that indicate the presence of sulphides. The concentration of chemosynthetic mussels, together with their estimated age based on shell size, indicates that these faunas developed after the slump failed. It was proposed by Tappin et al. (2001) that the size of the mussel shells indicates failure on 17 July 1998. By comparison, in the west, the clay exposed at the seabed in fissures and gullies is eroded. There is little evidence for recent movement, active venting, or the presence of chemosynthetic communities (see Fig. 2 in Tappin et al., 2001).

Originally, Amphitheatre morphology was interpreted from contoured bathymetry maps and ROV photographs, with the main features of the slump identified being a steep headscarp slope, with backward rotated fault blocks and a basal mound at the slump toe, formed by compression as the slump failed (Tappin et al., 1999; 2001). From that data set, the slump dimensions were set at 5 km long in a north-south direction and 7 km wide. Multichannel seismic (MCS) data (Sweet and Silver, 1999, 2003) confirmed the presence of slumping in the eastern Amphitheatre, with a maximum slump thickness of ∼760 m (labelled B in Fig. 2). The combination of MCS data and JAMSTEC/SOPAC bathymetry, led Sweet and Silver (2003) to reduce the width of the slump to 2.5–3.0 km, thereby calculating a slump volume of

3.8–4.6 km^3. The closely spaced grid of SCS data acquired in 2001 in the region of the Amphitheatre further delineated the 3-D architecture of the area (Tappin et al., 2003). Based on the SCS dataset, Tappin et al. (2003) increased the slump width to 6 km, with a corresponding increase in slump volume. However, we now recognise that the slump identified by Sweet and Silver (2003) in the east (B) is not part of the central, youngest, failure identified here as C. The seabed morphology proves that slump C truncates slump B on its western margin (Fig. 2). In addition, Tappin et al. (2003) included all three slumps as a single failure in their interpretation of the SCS data, hence the increase in width over that calculated previously. From our new interpretation we now recognise that within the Amphitheatre there are three slumps of different ages (A, B, and C) and that they are different failures.

Interpretation of the marine data set not only provides the morphology of the slump tsunami source and its relative age, it also allows us to explain the mechanism of failure. By inference, we can also account for the time lag between the earthquake and slumping. We have reported elsewhere that the slump may have been triggered by fluids driven upward by the main shock along secondary faults (Tappin et al., 2002). We hypothesise here that the most likely conduit for the water would have been the controlling normal fault, clearly imaged on the seismic data, which runs beneath the slump headscarp. The strongly reflective character of the fault on the MCS data suggests long-term active fluid movement leading to authigenic carbonate deposition along the fault plane (Fig. 3). This contrasts with the headwall fault imaged on adjacent MCS lines where the fault plane is not so sharply imaged suggesting a reduced level of authigenic carbonate precipitation (see Sweet and Silver, 2003). Authigenic carbonates were commonly observed on the surface of the central slump at the seabed intersection with the control fault under the headscarp (see Fig. 2, Tappin et al., 2001). The control fault is one of many along the inner trench wall, and is formed by subduction erosion, clearly a significant process acting along the margin (Tappin et al., 2001). On our new 3-D imagery, we locate the slump on the hanging wall of the control fault, across which we propose a pressure differential that acted as a pump for artesian water. The aftershocks, 20 min after the main shock, lie within the same general area as the control fault and slump. These may well have been caused by a similar differential pressure mechanism, although a shift in overburden pressure, caused by slumping, may have contributed. It is well documented that large landslides can generate earthquakes, a phenomenon called induced seismicity (e.g. Simpson, 1986). Slump displacement may have played a role in triggering the two aftershocks, especially because the shift in slump potential energy is much larger than the release of seismic energy by the two aftershocks.

6.2 New modelling of PNG

New simulation results (Fig. 4d), based on the new slump architecture, confirm the control of seabed morphology on a tsunami sourced from a location in the Amphitheatre. The results are in reasonable agreement with field observations. Generation and propagation of the tsunami as well as the resulting coastal runup are both controlled by the morphology of the Amphitheatre together with wave interactions with the Upraised Block. The Amphitheatre topography exerts an immediate influence on tsunami formation and propagation because of its similar size to the slump: the Amphitheatre is 10 km wide, compared to the tsunami wavelength of around 7.6 km. Consequently, the new slump architecture we identify here also has an important control on the tsunami source dimensions and, because of the Amphitheatre geometry, the runup results as well. Thus, it is important to identify the precise positioning of the tsunami source within the Amphitheatre. Different tsunami source positions within the Amphitheatre change where slump/Amphitheatre interactions initially occur, resulting in variations in the location and size of onshore runup (see Fig. 6 and Sect. 6.4.1). These results were produced on a uniform 100×100 m grid for the purpose of relative comparison.

The new tsunami simulations, based on a slump source timed from the m_b=4.4 aftershock at 09:02 and the T-phase records, are in good agreement (especially at Aitape) with accounts from survivors on timing, wave impact, and number of water waves (i.e. three) approaching the shore. They also explain the reports of the first wave breaking offshore, the simultaneous arrival of the wave with the aftershocks at Malol, and the wave converging onto Sissano Lagoon (see Davies, 1998). Figure 7 provides some specific examples of reproducing tsunami observations. One way to characterize simulation results is through wave breaking, as measured by the eddy viscosity localized on the front face of a breaking wave (see Chen et al., 2000). The maximum eddy viscosity is a measure of the strength of wave breaking, as well as a measure of wave nonlinearity. Strong wave breaking offshore (Fig. 7) explains the timing and location (3 km offshore) of the loud bang, and the northern horizon lit by the setting sun as reported by eyewitnesses on the sand spit before tsunami attack. Wave breaking also explains the highly localized erosional features observed on the lagoon side of the sand spit (Gelfenbaum and Jaffe, 2003). Figure 7 indicates that the first wave occurred more as a flood inundation, whereas the second wave was highly nonlinear throughout much of its inundation. These observations accord with the reports of survivors' located on the sand spit at the time of tsunami attack (Davies, 1998). The first wave propagated across Sissano Lagoon and entered the mangrove forest landward of the lagoon as a deep inundation by a large volume of water. The second wave did not penetrate the mangrove forest as far inland, but maintained strong wave breaking throughout inundation, as reported by survivors carried into the forest by that wave

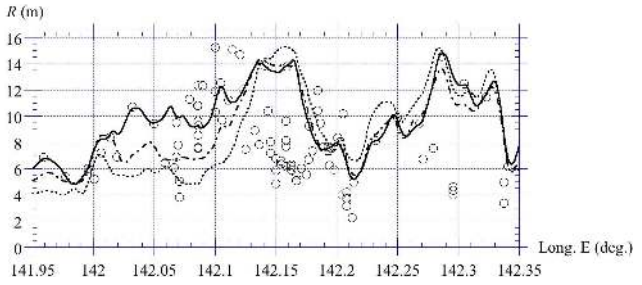

Fig. 6. Comparison of maximum runup results for the tsunami source trough located at longitude and latitude: dotted line (142.25820 E, 2.87910 S), dashed line (142.25455 E, 2.86100 S), and solid line (142.25090 E, 2.84290 S). The tsunami source is being shifted downslope, along the axis of failure, by 2 km and 4 km, which corresponds closely to a quarter and half wavelength, respectively. The comparison is carried out with a uniform 100×100 m grid spacing.

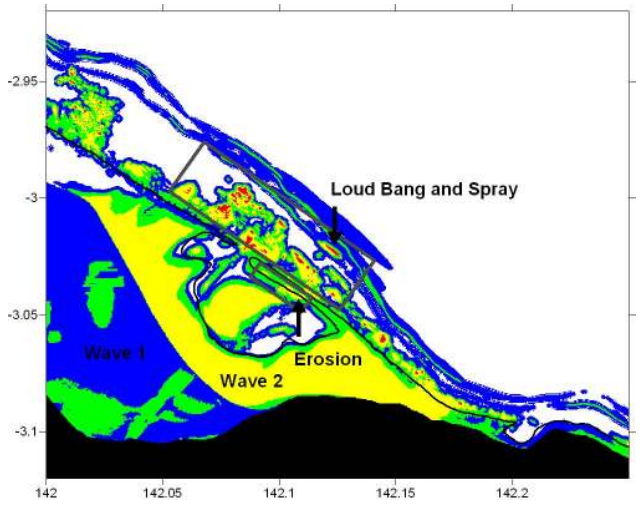

Fig. 7. Results from our new Boussinesq simulation carried out with a uniform 50×50 m grid spacing. Map of maximum eddy viscosity υ (as defined in FUNWAVE) localized on the front face of breaking waves: blue [very mild, υ=0.01], green [mild, υ=1], yellow [strong, υ=9], red [very strong, υ=40]. Regions of strongly nonlinear breaking waves and bores (yellow and red) are seen both offshore and onshore. A complex pattern occurs onshore from three different incident waves. See text for further discussion.

(Fig. 7). The results from our numerical tide gauges (Fig. 8) located in shallow water next to the villages of Malol and Aitape match the reported time of tsunami arrival, relative to the aftershocks, in both villages. At Aitape, the absolute time of tsunami arrival, two minutes early in our simulation is explained by the offshore location of the numerical tide gauge relative to the village.

Our modelling shows the tsunami striking Malol at the same time as the aftershocks, a relationship that provides an explanation as to why the aftershocks were not reported by the survivors at this location. It also explains the reports from survivors' on the sand spit who remembered the tsunami striking after the aftershocks, because the wave swept across the sand spit between 21.6 and 24.7 min after the earthquake (Fig. 5d–f). One of the most significant features of our new wave propagation results is the correspondence with survivor evidence from Aitape that the tsunami struck at 09:15 GMT, 25 min after the earthquake (see Fig. 5g). Our simulated wave arrives within one or two minutes of the time reported from this location (Davies, 1998). The simulation also shows that the tsunami strikes Arop village after striking Malol, contrary to some previous reports (Davies et al., 2003; Synolakis et al., 2002). This sequencing can be explained by the offshore morphology. The Yalingi Canyon extends offshore of Malol, and within its relatively deeper waters, as mentioned above, the tsunami waves travel faster than elsewhere (see the wave fronts on Fig. 5a–d).

The offshore morphology also explains the apparent anomaly of runup around Malol. Based on dead reckoning from the slump location, there should have been maximum runup at Malol, because the village is directly in line with the axis of slump motion. In fact, however, the runup at Malol is less than at other villages to the immediate west, such as Arop, which was completely devastated. This apparent anomaly can be explained by wave energy being refracted away from Malol and onto the shelf off Sissano, because of the relatively deeper water of Yalingi Canyon (Tappin et al., 2001). The canyon is therefore responsible for both the first tsunami arrival at Malol, as well as the much smaller amplitude tsunami experienced here.

West of Malol and Arop, the Sissano and Arnold areas were the last to experience tsunami attack, as seen by the wave travelling westward and refracting around the Bliri Headland (Fig. 5g–h). The morphology of the Arnold River delta explains why tsunami waves were focussed onto Sissano Lagoon, resulting in maximum runup there. The tsunami focussing was the result of the hemispherical shallow water shelf that forms the offshore extension of the Arnold River delta (Tappin et al., 1999; Matsuyama et al., 1999; Heinrich et al., 2000). The shallow delta also causes the tsunami to arrive at Sissano and Arnold later than the other impacted villages to the east. Once again, geological features control tsunami observations.

6.3 Advances in tsunami modelling

Two of the main scientific advances resulting from investigations into the cause of the PNG tsunami are: 1) the development of new modelling methodologies to address SMF tsunami sources, and 2) the improved recognition of the significant differences between modelling earthquake tsunamis as opposed to SMF tsunamis. Because of the importance of modelling in assessing tsunami hazard, we review the main phases of model development over time.

6.3.1 Onboard Kairei modelling – 1999

The first numerical simulation of the slump devised onboard the *Kairei* (Fig. 4a) was rudimentary, with many assumptions not yet validated. There was no slump (as opposed to landslide or sediment flow or slide) tsunami generation model available. Initial tsunami generation estimates were computed by hand, based on published (or soon to be published) literature (Watts, 1998, 2000; Grilli and Watts, 1999). The slump architecture was provisional and based only on the bathymetric data acquired during the initial survey (Tappin et al., 1999). Slump dimensions were 7 km wide, 5 km long, and 200 m thick. The slump failed down a slope of mean gradient 12°, and horizontal slump movement was 3–4 km towards an azimuth of 345°. The initial water depth of the slump centroid was 1400 m.

The tsunami source, based on a solid block 2-D underwater landslide model (Grilli and Watts, 1999) did not use depth-averaging. Instead, the source solved fully nonlinear potential flow (FNPF) equations, which allowed for vertical water acceleration. The tsunami simulation however used linear shallow water wave equations. The maximum wave height of 6 m was located offshore of the sand spit, with wave heights measured at the 10 m water depth contour (Fig. 4a). Although approximating the relative distribution of runup along the coast, the maximum offshore water height was not of the same magnitude as runup measured by the onland surveys. A key result of the simulation was significant wave heights west of the lagoon (published in Tappin et al., 1999). These wave heights occurred because of wave interactions (i.e. reflection, diffraction, refraction, etc.) with the Upraised Block and proved that the tsunami could only be sourced from within the Amphitheatre.

An earthquake source was also modelled, located along the 40-km Fault, on the assumption that this was a thrust fault (although the authors were aware that it was not). The simulation was based on linear depth-averaged long wave equations (published later in Matsuyama et al., 1999). For a shallow dipping thrust, there was a maximum wave height of up to 2 m offshore of the Sissano sand spit. For the steeply-dipping alternative, the maximum wave height was 8 m, although the offshore wave height distribution did not correlate well with the measured onshore runup (Tappin et al., 1999; Matsuyama et al., 1999). Comparing the results of the modelling, it was the slump, rather than the earthquake, that was the more likely tsunami source, although it was obvious that further marine surveys and further refinements of slump modelling were required to validate this interpretation.

6.3.2 Post cruise tsunami modelling – 2001

The second simulation developed after the surveys (Tappin et al., 2001; Watts et al., 1999) was a major advance over that derived onboard the *Kairei*. It was based on a slump mechanism of SMF motion, that was approximated by a rotational failure similar to that of a damped pendulum. The slump architecture was better defined than previously because of access to the MCS data of Sweet and Silver (1999). A slump volume of 4 km^3 was based on slump dimensions of 4 km width, 4.5 km length (revised from the multibeam data) and 600 m thickness. The sediment physical properties were based on the sediment cores acquired during the marine surveys.

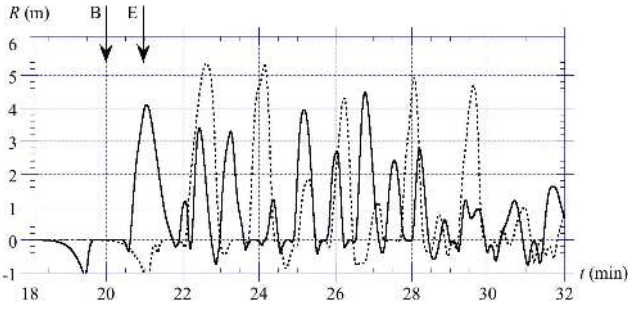

Fig. 8. Numerical tide gauges located in shallow water next to the villages of Malol (solid line), and Aitape (dashed line). The time of tsunami arrival relative to the aftershocks (B for "beginning" and E for "end" between 20 and 21 min after the earthquake) is correct at Malol although two minutes early at Aitape, because of the location of the numerical tide gauge relative to the village.

A slump basal shear strength of Su=0.8 MPa, or a Coulomb friction coefficient of Cn=0.11, was found to reproduce the slump displacement of ∼1 km. These values gave a slump initial acceleration of a_o∼0.51 m/s^2, and maximum velocity of ∼23 m/s. To solve the equations of fluid motion, the centre of mass motion was incorporated as a boundary condition into a FNPF simulation of tsunami generation (Grilli and Watts, 1999), in which the slump was represented by a semi-ellipse. The simulation showed the continual growth of tsunami amplitude during the first 44 s of slump acceleration, which ceased as the waves propagated outwards. (Note: 44 s corresponds to the characteristic time of slump motion t_o, found to be identical to the duration of slump acceleration, as well as identical to the tsunami wave period (Grilli and Watts, 2005).) Tsunami generation was therefore chosen to take place over t_o=44 s.

Because there were no validated 3-D models available to predict the evolution of the free surface in the transverse direction, the 2-D simulation result was transformed into a 3-D tsunami source using mass conservation considerations along the third dimension. The transverse wave profile was thus represented by a function $sech^2\{3(y-y_0)/(w+\lambda)\}$, with the slump width w=4 km, and the characteristic tsunami wavelength λ=4.4 km. The factor of 3 was chosen to yield a relative wave amplitude of 1% at the transverse distance $y-y_0=w+\lambda$, where y_0 is at the centre of the slump location. By carrying out the conservation of mass calculation, the PNG slump dictates a 2-D to 3-D reduction of $w/(w+\lambda)\approx 0.5$ in the initial tsunami amplitude, due to transverse wave propagation during tsunami generation.

The 3-D tsunami source predicted at 44 s provided the basis for simulations of propagation and inundation performed with TUNAMI-N2 (see Imamura and Goto, 1988). The mathematical expression of the sea surface shape at time t_o was given by:

$$\eta(x, y) = sech^2\left(\frac{3(y-y_0)}{8.4}\right)\begin{pmatrix} -35.71\exp(-0.1013(x-29.07-x_0))^2 \\ +25.14\exp(-0.05169(x-31.71-x_0))^2 \end{pmatrix}$$

which transferred the tsunami source from the generation model to the propagation model. Water velocities were neglected, because there was no numerical interface available to link the two models at that time. The bathymetry was a compilation of the *Kairei* swath data at depths greater than 400 m, and data from the shoreline to 150 m interpolated from the Aus. 389 chart. Intervening depths between 150–400 m were merged by linear interpolation. Onland topography around Sissano Lagoon was based on transects acquired by the field surveys (Kawata et al., 1999). Because of the poor resolution of the nearshore bathymetry, and the uncertainty of the effects of the interactions between shoaling waves with the shallowest regions fronting Sissano Lagoon, a uniform grid spacing of 200 m was used for the bathymetry. The correlation between the measured runup and simulated wave heights was, however, found to be quite good (Fig. 4b and Tappin et al., 2001), although the highest waves occurred several kilometres offshore. Because of limitations of the wave propagation model TUNAMI-N2 this second simulation still only yielded offshore wave heights, instead of actual onland runup. We return to this below. There were many assumptions made in deriving the tsunami source based on FNPF simulations, and then transforming the source from 2-D to 3-D. (These techniques were validated later (see Watts et al., 2003, 2005a; Grilli and Watts, 2005; Enet and Grilli, 2003, 2005, 2007).)

Heinrich et al. (2000) may have been the only other early publication on the tsunami source to apply methods comparable to those of Watts et al. (1999) and Tappin et al. (2001). Their landslide simulation was based on a translational SMF of cohesionless granular material, not a slump. Using the *Kairei* bathymetry and a landslide volume of 4 km^3, they achieved a close correlation with the measured runup along the coast. Modelling of the alternative earthquake sources (shallow or steeply dipping thrusts) could not explain the measured runup. Synolakis et al. (2002) applied a similar methodology to that of Watts et al. (1999) and Tappin et al. (2001). They discounted the steeply dipping thrust mechanism on seismological grounds, and modelling of the shallow dipping thrust as a tsunami source yielded maximum wave heights of 40 cm. The only significant difference to the modelling of Tappin et al. (2001) is their use of the MOST model of tsunami propagation and inundation, which solves the same nonlinear shallow water wave equations as TUNAMI-N2, but with the method of characteristics (Titov and Synolakis, 1998). Following Tappin et al. (2001), they concluded that the slump in the central region of the Amphitheatre was the source of the local tsunami. As with other simulation models, using MOST gave offshore maximum wave heights, because onland runup was minimal or not present in the simulation. This fact motivated our new simulations of the PNG event with a Boussinesq water wave model.

6.3.3 Recent modelling

The first of our Boussinesq simulations used our previous slump dimensions and was published in Watts et al. (2003) (Fig. 4c). A uniform 100×100 m bathymetry grid spacing was used. The second of our Boussinesq simulations, prepared for this paper, is based on the new slump architecture described above (Figs. 2 and 3). Compared with earlier modelling work, these simulations benefited from a validated and better understood 3-D tsunami source (Grilli et al., 2002), and the use of a finer 50×50 m grid spacing for wave propagation and inundation (Fig. 4d).

Much of the early work on slumps has since been validated and verified. With regard to tsunami generation, the previously assumed slump basal shear strength of $S_u \approx 0.8$ MPa, and Coulomb friction coefficient of $C_n \approx 0.11$, were considered to be unrealistically high compared to available published values (e.g. Imran et al., 2001). These shear and friction values are now validated for slumps (Watts and Grilli, 2003; Watts et al., 2005a) even though the values are greater by one to two orders of magnitude than those of most translational landslides. The equation of SMF motion previously applied (see Watts et al., 1999, 2002) was fully derived, experimentally validated, and the secondary effect of SMF deformation on tsunami generation quantified (Grilli et al., 2005; Watts et al., 2005a; Enet and Grilli, 2007). The transformation of a 2-D to a 3-D tsunami source, using mass conservation considerations along the third dimension, was fully supported by 3-D numerical experiments, and validated by large-scale 3-D laboratory experiments (Watts et al. 2005a; Grilli et al., 2002; Enet et al., 2003, 2005, 2007). The improved 3-D tsunami source incorporates both transverse propagation and initial water velocities.

With regard to tsunami propagation and inundation, FUNWAVE is a fully nonlinear and dispersive long wave "Boussinesq" model that features an accurate moving shoreline algorithm and energy dissipation terms (Wei and Kirby, 1995; Wei et al. 1995; Chen et al., 2000; Kennedy et al., 2000). The use of FUNWAVE for tsunami simulations has been well validated by case studies, based on a pyroclastic flow (Waythomas and Watts, 2003), underwater landslides (Watts et al., 2003; Day et al., 2005; Greene et al., 2005), earthquake generated tsunamis (Day et al., 2005; Grilli et al., 2007; Ioualalen et al., 2006, 2007), and a debris flow (Walder et al., 2005). The inclusion of both nonlinear and dispersive terms in Boussinesq models eliminates the excessive shallow water steepening, and corresponding early offshore wave breaking and dissipation, that take place in NSW wave

models (such as TSUNAMI-N2 or MOST) and hence allows for tsunami runup to occur onshore. The frequency dispersion in the model is also necessary to account for the shorter wavelengths of SMF tsunamis, which have horizontal water velocity profiles that vary with depth. The improvements in modelling resulting from the use of FUNWAVE led, for the first time, to tsunami runup occurring onland in the simulations, rather than as offshore wave heights.

6.4 Uncertainty in simulated tsunami runup

Our new work raises fundamental questions about some of the many factors that affect the alongshore runup distribution predicted in numerical simulations, their correlation with observations on runup, and controls on the incidence of tsunami waves striking the coast. These factors include the tsunami simulation itself, the reliability of the onshore measurements, and our understanding of wave interactions with other waves and with the shoreline.

6.4.1 Grid refinement

Comparison of our latest simulated runup with measured runup still shows some differences that remain unexplained (Fig. 4d). To demonstrate the sensitivity in the positioning of the tsunami source in relation to the Amphitheatre morphology and location of the Upraised Block, we simulated several different tsunami source positions along the slump axis of failure on a 100×100 m uniform grid (Fig. 6). The slump centroid is located at longitude and latitude (142.2582 E, 2.8791 S) and, based on experimental results (e.g. Enet and Grilli, 2007), the deepest trough of the tsunami source is usually positioned above this location. We also ran simulations with the deepest trough located at (142.2546 E, 2.8610 S), and (142.2509 E, 2.8429 S), respectively downslope at, 2 km or one-quarter wavelength, and 4 km or a half wavelength. As the tsunami source moves towards the Upraised Block, more wave energy is directed to the west side of Sissano Lagoon and the region of highest runup is extended farther west. The simulated runup could potentially converge onto a unique slump location that reproduces measured runup (see Heinrich et al., 2000), but we do not carry that process any further here.

We should note, however, that the runup measurements themselves may be suspect. Borrero (2001) questioned what runup actually represents, and discussed the inherent problems in its measurement (e.g. differentiating between flow depth, runup, and wave splash). On the one hand, observers of the PNG event indicate that many trees were bent over by the tsunami waves, which would thereby increase the height of the apparent runup measured during post-tsunami surveys, by the location of objects caught in trees, as well as by the stripping of foliage. It was reported that water forces were strong enough to strip almost all branches off *Casurina* trees along the coastline below a certain height (Kawata et al., 1999), a fact observed first hand by two authors (DRT and PW). On the other hand, subgrid wave interactions (i.e. here, on scales less than 50 m) and splash would make simulated results underestimate runup measurements. There is no known technique to assess and balance these contrary effects. There is also the presence (or absence) of measurable features of sufficient height, by which peak runups may be measured, that might bias results. It is not inconceivable that the tsunami runup peaked at +20 m (see Fig. 4d), but the evidence for this height was not preserved. The correlation in Fig. 4d between simulated and measured runup is as good as we can expect from a first hand simulation made without iterations or adjustments.

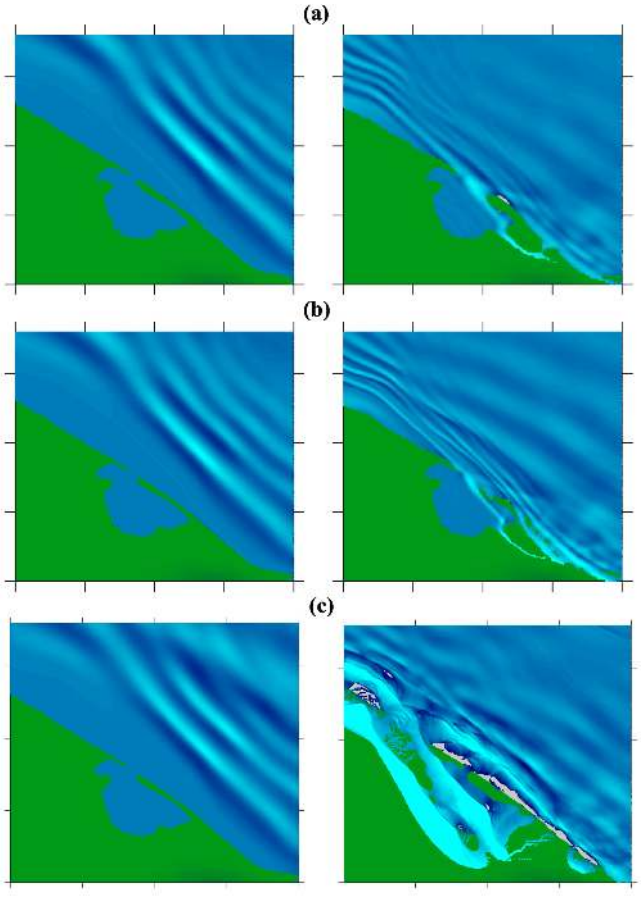

Fig. 9. A sensitivity analysis of our new Boussinesq simulation with respect to grid spacing. Snapshots of the free surface are shown at 18.8 min (left) and 23.8 min (right) after the main shock for: **(a)** uniform 200×200 m grid spacing, **(b)** uniform 100×100 m grid spacing, and **(c)** uniform 50×50 m grid spacing. See text for further discussion.

Simulation results depend on the bathymetry data, the choice of simulation model, and the simulation grid spacing. Figure 9 compares free surface snapshots of FUNWAVE results obtained with the same tsunami tsunami source on 200 m, 100 m, and 50 m uniform bathymetry grids. Prior to

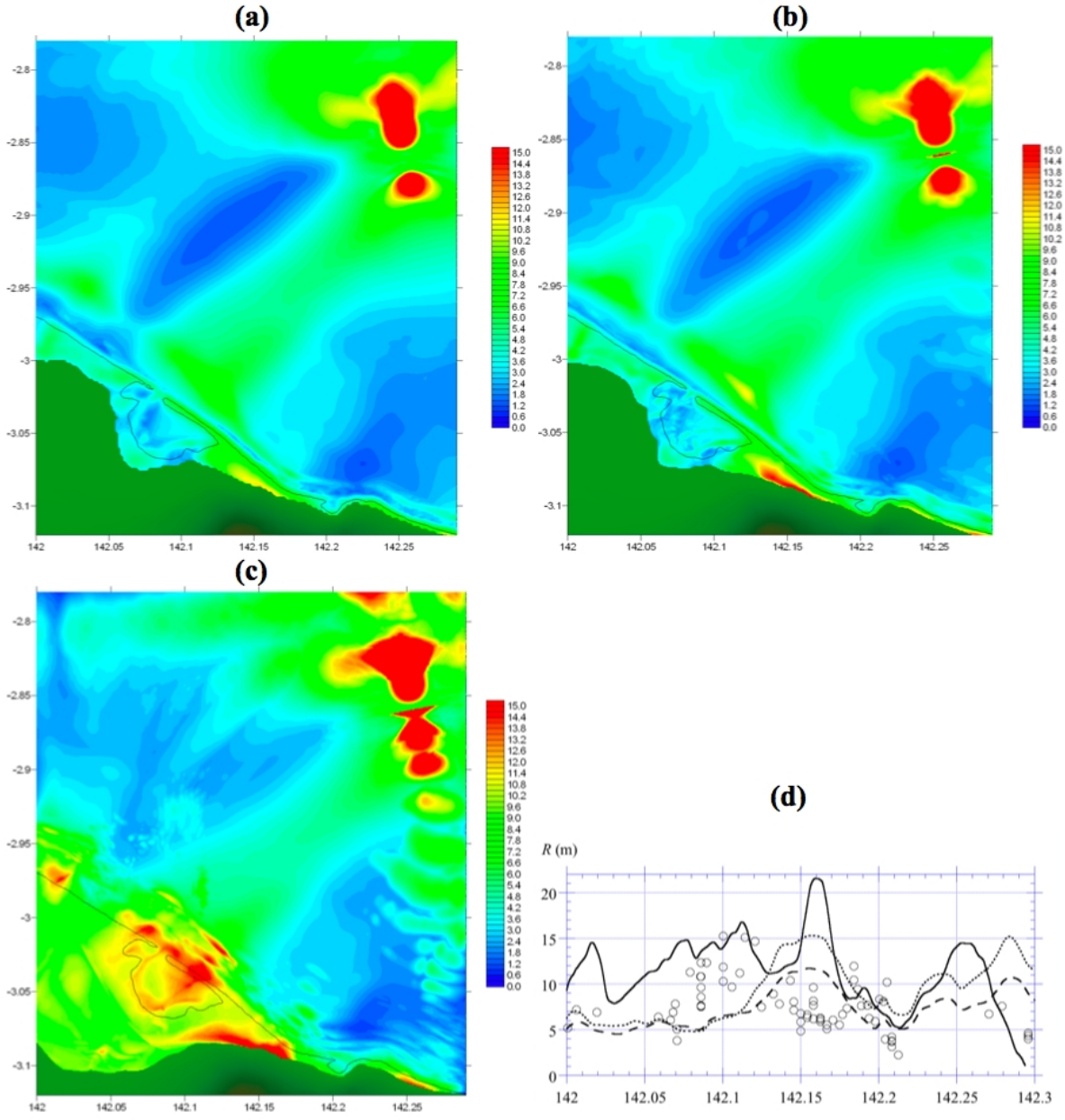

Fig. 10. A sensitivity analysis of our new Boussinesq simulation with respect to grid spacing. Maximum water elevations at any time during the simulation are provided for: **(a)** uniform 200×200 m grid spacing, **(b)** uniform 100×100 m grid spacing, and **(c)** uniform 50×50 m grid spacing. **(d)** Comparison of onshore runup for the three grid spacings. Dashed line – 200 m, dotted line – 100 m, solid line – 50 m, and circles – measured runup. See text for further discussion.

interactions with the shoreline, the shoaling wave appears nearly identical. However, the simulations performed with larger grid spacing either dissipate or reflect wave energy, limiting the water volume on land and slowing the speed of tsunami inundation. Figure 10 compares the maximum wave elevations at any time during the simulation, as well as simulated and measured runup. The maximum wave elevations above sea level produced with a 50 m grid display the full complexity of wave breaking, edge wave interactions, and the inundation of multiple waves (Fig. 10c). The difference in simulation results from the onset of inundation and onward is significant (Fig. 10d). A similar sensitivity analysis was carried out by Ioualalen et al. (2007) for the 26 December 2004 tsunami striking Thailand, where a uniform 460×460 m grid was necessary to capture the wave dynamics for a large earthquake tsunami. The shorter wavelength of an SMF tsunami requires a smaller grid spacing.

6.4.2 Beach slope

With regard to the beach slope (in a 2-D vertical plane), NSW wave theory predicts that this is an important control on tsunami wave runup (e.g. Kanoglu and Synolakis, 1998). Using Boussinesq modelling for the PNG event, we can actually model onshore runup rather than offshore tsunami wave heights. Hence, we had an opportunity to investigate whether this prediction is borne out. A constraint on our modelling is undoubtedly the poor nearshore bathymetric control in water depths shallower than 400 m that may compromise any conclusions we can draw on this subject. However, for PNG, we do know that runup involved short wavelength breaking waves and bores. For example, most eyewitness accounts from the sand spit describe either a wave breaking on the beach, or a vertical wall of water that was probably a bore. Our latest simulation shows that some waves broke several kilometres offshore, again near the shoreline, and once more on the landward side of the sand spit (Fig. 7). In this kind of dynamic wave environment, with rapid evolution of relatively short wavelength waves, we consider it unlikely that runup predictions based on NSW wave theory are relevant to tsunami runup during the PNG event. We therefore question the relevance of beach slope effects on the runup results and, in the instance of PNG, consider it not as important as previously predicted.

6.4.3 Edge waves

Numerical simulations of other tsunami events using FUNWAVE (e.g. Day et al., 2005; Greene et al., 2005; Ioualalen et al., 2007) suggest that maximum inundation and maximum runup may be caused at some locations by collisions (or interactions) of edge waves travelling in opposing directions along the shoreline (Watts et al., 2003; Waythomas and Watts, 2003). Despite being present in our previous simulation results, edge wave interactions have received little attention in the context of tsunami hazards, specifically with regard to maximum runup. Whereas, during the PNG event, most of the sand spit experienced oblique wave attack, edge waves appear to have played a role in causing maximum runup around Aitape, the entrance to Sissano Lagoon, and the mouth of the Arnold River. In all of these locations, simulations show that edge waves travelling in opposite directions interact with each other thereby producing peaked wave heights and maximum runup long after most other locations along the coast had ceased experiencing dangerous wave activity (see Figs. 4d, 7, and 9c). Clearly, the tsunami hazard from edge wave interactions is very local. However, the locations of such interactions remain unpredictable without detailed modelling, and the interactions themselves are highly three-dimensional. In the presence of interacting edge waves, there can be no simple 2-D estimates of maximum tsunami runup, based on vertical planar transects. The runup hazard is intrinsically three-dimensional for all tsunamis.

6.4.4 The important choice of wave equations

A method of assessing the relative importance of nonlinear and dispersive effects during water wave propagation is the Ursell number; the ratio of nonlinear to dispersive effects of a water wave. Table 1 shows ratios of tsunami amplitude a to depth h, and tsunami wavelength λ to depth h, as well as the Ursell number $U = a\,\lambda^2 / h^3$ for selected locations along a straight transect from the slump to the sand spit in front of Sissano Lagoon. Based on these values, especially the Ursell number, wave breaking could have been expected during tsunami propagation on the shallow shelf in front of Sissano Lagoon (Watts et al., 2003). The values in Table 1 suggest that all modelling capabilities of FUNWAVE were required if we were committed to reproducing all of the tsunami observations, from generation through propagation to inundation. While the numbers in Table 1 were derived from our simulation, they can be estimated from engineering approximations prior to an event (Watts, 1998, 2000; Watts et al., 2005), and clearly guide the choice of an appropriate simulation model. Enet and Grilli (2007) used similar estimates to design 3-D SMF experiments.

Dispersive effects in the PNG event play specific roles during shoaling and breaking/dissipation of tsunami waves. Figure 11 illustrates these considerations by comparing dispersive and non-dispersive simulations of the PNG event (made here by running FUNWAVE in non-dispersive mode) using our latest slump tsunami source. We see that the NSW simulation overpredicts wave focusing and shoaling in the shallow water area fronting Sissano Lagoon (Fig. 11a), where waves build up early to a maximum of around 18 m in amplitude (Fig. 11c) and then rapidly attenuate through numerical dissipation before reaching the shore with a much reduced wave height. By contrast, in the dispersive simulation, breaking and dissipation occur closer to the shoreline (Fig. 11a). In addition, Fig. 11b shows that the Boussinesq model captures the three elevation waves observed by survivors, whereas the NSW model, lacking dispersion, produces only two elevation waves, one for the tsunami source itself and a smaller wave for its rebound at the source. Since both simulations used the same discretization scheme, moving shoreline algorithm, wave breaking algorithms, and 50×50 m grid, results in Fig. 11 independently assess the effects of dispersion on model results. We note a fundamental failure of the NSW wave equations present in NSW simulations carried out with FUNWAVE, TUNAMI-N2, and MOST. Simulations of the PNG event appear to need dispersive wave equations to achieve realistic and accurate results. Of course, this result is not generally true for all tsunamis. For instance, recent simulations by Ioualalen et al. (2007) of tsunami impact in Thailand during the 26 December 2004 event showed that dispersion affected runup values very little, which was expected given the longer wavelength of earthquake tsunami waves. Indeed, we found nearly identical NSW and Boussinesq simulation results for the earthquake tsunami generated

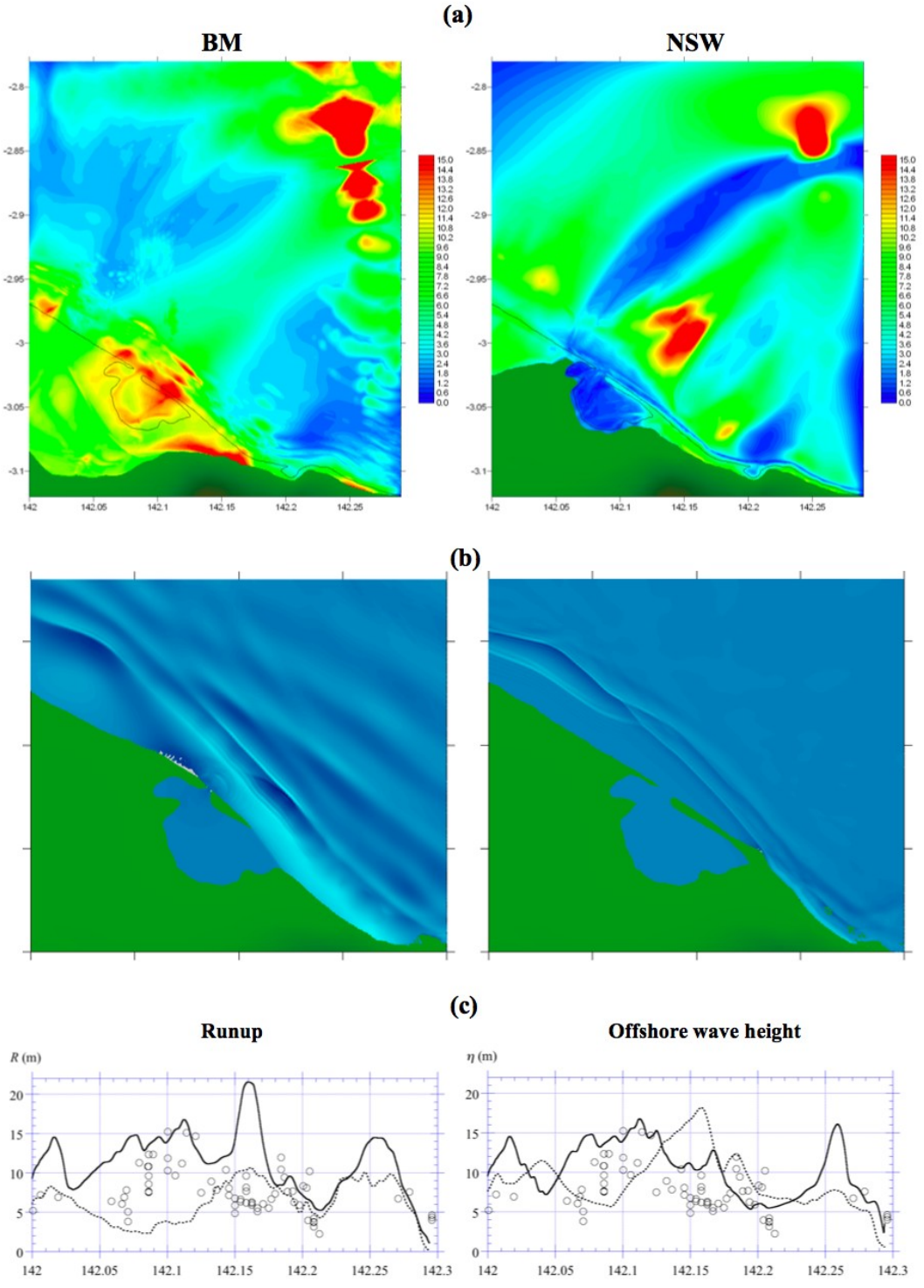

Fig. 11. A comparison of results from the Boussinesq and NSW models of FUNWAVE for identical discretization scheme, bathymetry grid, uniform 50×50 m grid spacing, and tsunami source. **(a)** Maximum water elevations at any time during the simulation. The large amplitude wave in front of Sissano Lagoon in the NSW model is an anomalous feature. **(b)** Snapshot of the free surfaces at 21.3 min after the main shock. The NSW model produces one sharp N-wave and a smaller wave from rebound at the source, with high frequency numerical instabilities, especially during interactions with the shoreline. **(c)** Comparison of maximum offshore wave heights, and comparison of onshore runup along with measured runup (circles). Dotted line – NSW, solid line – Boussinesq. The offshore wave heights give the NSW model an appearance of reproducing tsunami runup, although the actual runup results fall well short of the onland measurements. See text for further discussion.

Table 1. Wave parameter values during tsunami propagation from source to shore.

Distance from shoreline (km)	a/h	λ/h	$U=a\,\lambda^2/h^3$	Nonlinearity	Dispersivity
Source (25)	0.0093	2.4	0.056	Mildly	Fully
21	0.0078	4.8	0.18	Linear	Mildly
14	0.0092	7.9	0.57	Linear	Mildly
5.6	0.046	23	24	Cnoidal	None
2.8	0.34	60	1200	Breaking	None
1.0	0.60	160	15000	Breaking	None

by the main shock during the PNG event.

Lynett et al. (2003) also ran a successful Boussinesq simulation of the 1998 PNG event although they did not attempt to reproduce all tsunami observations (see Sect. 6.5). Notwithstanding, they made the surprising claim that a NSW model was necessary to reproduce the overland inundation correctly, a claim that contradicts the results of Tappin et al. (2001), Synolakis et al. (2002), as well as the results presented here. With its accurate inundation algorithm on dry land, using a slot method, FUNWAVE has successfully reproduced coastal inundation for all tsunami events studied to date (see Watts et al., 2003, 2005b; Waythomas and Watts, 2003; Fryer et al., 2004; Day et al., 2005; Ioualalen et al., 2007). The choice of numerical model is thus critical in reproducing data acquired by onshore field surveys and from survivor observations. Whereas Boussinesq simulations may not have been possible in the past due to their more computationally intensive nature, this is no longer the case, and our results for PNG confirm their importance for tsunamis generated by SMFs.

6.5 Ramifications of our new understanding

During our continuing study of the PNG event, we have progressively improved our understanding of the general controls on tsunami generation by SMF. Based on this research, we can make a number of observations regarding SMF tsunami generation that are of more general consequence.

It has been proposed that SMF tsunami sources can be represented by dipoles (Okal and Synolakis, 2003), i.e. the equivalent of two instantaneous volumetric fluxes placed in close proximity. Our research, however, shows that the generation of a tsunami by a moving SMF occurs over some finite region of space and (in contrast to earthquakes) over a relatively long time (t_0) related to SMF kinematics, during which time the leading elevation wave can travel a significant distance before a trough is formed (Grilli and Watts, 2005). The elevation wave behaves like a volumetric flux positioned ahead of the SMF, whereas the trough above the SMF behaves like an equivalent volumetric flux of opposite sign (i.e. an absence of water). This tsunami generation mechanism results in two volumetric fluxes situated widely apart – instead of a dipole. The experimental results of Wiegel (1955) and Watts (1997, 2000) demonstrate that the leading wave of a tsunami generated by a SMF propagates as if the source were volumetric. (While these experiments were carried out along 1-D channels, we note that the conclusion of volumetric wave propagation is general and applies equally well to 2-D radial geometries.) Hence, the asymptotic tsunami behaviour in the far field is not that of a dipole. Therefore, we conclude that tsunamis generated by SMFs cannot be represented as simple dipoles. This new understanding on the basic mechanism of SMF tsunami generation leads to the logical conclusion that the leading elevation wave will have a far greater tsunami potential in the far field than previously believed. In scaling terms, assuming radial spreading in a constant depth ocean, the far field tsunami amplitude would decay as $1/r$ for a volume, instead of $1/r^2$ for a dipole, where r is the radial distance from the tsunami source. The implication is that the SMF tsunami in the PNG event may have contributed to the earthquake tsunami in the far field, including in places like Japan. While it is not our purpose here, we point out that this hypothesis can be tested.

Some researchers have used a single constant SMF velocity to describe tsunami generation (e.g. Tinti et al., 2001; Ward, 2001; Okal and Synolakis, 2003). Recent work demonstrates that tsunami generation takes place essentially during the *initial* phase of SMF acceleration, during which time the instantaneous velocity is approximated by $u\,(t) \approx a_o\,t$. Therefore, with SMFs, there is no characteristic velocity that can be used to describe their motion, and their initial acceleration is the only relevant parameter to describe their motion during the tsunami generation phase (Enet and Grilli, 2007; Grilli and Watts, 2005; Watts et al., 2005a; Watts, 1998). Further discussion of this issue can be found in Greene et al. (2005) and Watts et al. (2005a).

Regarding the maximum velocity attained by a SMF, we show that this is dependent on the size of the failure together with the local seabed morphology (Grilli and Watts, 2005). In the instance of PNG, our results indicate the slump reached a maximum velocity of around 15 m/s near the middle period of motion, which lasted in total approximately 100 s. Assuming the same size slump, a smaller maximum

velocity would require less displacement down the slope, whereas a greater maximum velocity would require more displacement. The slump displacement therefore constrains the slump velocity. Maximum SMF velocity is highly sensitive to the geology, downslope displacement, and the SMF size. Large translational slides on long continental slopes can have much higher centre of mass velocities (e.g. Fryer et al., 2004; Waythomas et al., 2008[1]).

6.6 Earthquake versus SMF Tsunami Sources

Our work also has important ramifications for understanding the differences between tsunamis generated by SMFs and earthquakes, an understanding that has in large part been validated by work since 1998. Both earthquakes and SMFs involve vertical sea floor movement that affects the water column and results in gravity driven displacements of the sea surface that spread out as waves from the source. For an earthquake source, the initial tsunami wave field is determined primarily from the vertical coseismic displacement field of the seafloor, which is a measure of earthquake magnitude (Hammack, 1973; Geist, 1998). For the rise time of most earthquakes, the long-wave phase velocity in the ocean is slow enough so that the displacement is usually considered instantaneous. (In this respect, the 9.3 magnitude earthquake of 26 December 2004 in the Indian Ocean, which had an extremely large rupture/source area, was an exception; e.g. Grilli et al., 2007.) Because of the relatively large source area of most earthquakes, the resulting vertical seafloor deformation usually (but not always) generates a tsunami with longer wavelengths and longer periods compared to those generated by SMFs (Hammack, 1973; Watts, 1998, 2000). The tsunami generated is thus mainly dependent on the earthquake magnitude, together with centroid mechanism and depth (Hammack, 1973; Geist, 1998b), except in instances where the earthquake is "slow" (Kanamori, 1972; Newman and Okal, 1998b). Coseismic displacement generates tsunami amplitudes that rarely exceed 10 m at the source (which was the case for the 26 December 2004 tsunami; e.g. Grilli et al., 2007).

In contrast to earthquakes, SMFs usually take place more slowly and at slower dislocation velocities (Grilli and Watts, 2005; Watts et al., 2005a). The longer source time reduces the efficiency with which a tsunami is generated, and allows the source to spread in area during tsunami generation. However, a relatively shallow depth SMF (i.e. submergence to length ratio) can more than compensate for the longer source time in terms of tsunami generation (Grilli and Watts, 2005). Given the potential for large SMF displacement and size, tsunami amplitude does not have a *theoretical* upper bound other than the water depth itself. Despite spreading during generation, the tsunami source area above a SMF is usually much smaller than that of an earthquake source. There is also a strong directivity along the SMF axis of motion (Iwasaki, 1997; Fryer et al., 2004; Enet et al., 2003, 2005, 2007; Waythomas et al., 2008[1]) that often results in focused local runup (Imamura and Gica, 1996; Imamura et al., 1995), the magnitude of which is a function of tsunami source location, initial wave amplitude, and wavelength.

Another complication in the generation of tsunami by SMF is the variety of their failure mechanisms. As a simplification for modelling purposes, two end members of SMF were recognised (Grilli and Watts, 2005): (1) slumps, which fail while largely maintaining their structural integrity; and (2) landslides, which are translational and often evolve morphologically during failure. The composition of the SMF determines its law of motion, from which the tsunami source is derived. The law of motion therefore controls tsunami generation and tsunami magnitude (Grilli and Watts, 2005). Landslides initiated in shallow water and travelling down the continental slope can be tsunamigenic over considerable distances. In contrast, slumps typically do not travel as far as landslides because of basal friction, thereby reducing their potential in generating tsunamis. Thus, SMFs may result in tsunamis with amplitudes limited only by the vertical extent of their centre of mass displacement (Murty, 1979; Watts, 1998), which can potentially reach several kilometres in magnitude, as in large-scale volcano flank failure (e.g. McMurtry et al., 2004). Hence, despite the smaller SMF source area, both mass failure centre of mass motion and the subsequent tsunami amplitude at the source can surpass those of coseismic displacement by several orders of magnitude (Schwab et al., 1993; Watts, 1998).

6.7 The controversy

The roots of the controversy over the source of the PNG tsunami stem from the fact that in 1998 SMFs were mainly considered in terms of translational events. The modelling of translational events either did not produce tsunamis with significant local runup, and/or with simulated runup that matched measured runups. Thus, for some scientists, a SMF mechanism was ruled out, and the earthquake was, almost by default, considered the only possible tsunami source. It was on the basis of such an argument that the steeply dipping thrust mechanism was identified by some authors (e.g. Kikuchi et al., 1999) as the preferable earthquake rupture mechanism and thus used to explain the tsunami. This choice of rupture was made even though the earthquake mechanism was more likely to be a shallow dipping thrust (McCue, 1998; Heinrich et al., 2000). Key to the slump tsunami source is the runup west of Sissano Lagoon that can only be explained by a source located within the Amphitheatre, as reported early on by Tappin et al. (1999).

Submarine slumps are rare, at least compared to other SMFs. Thus, even when the marine data identified a slump offshore of Sissano (Tappin et al., 1999), this geological fact was ignored (e.g. Matsuyama et al., 1999; Geist, 2000; Iwasaki and Satake, 2001; Satake et al., 2003). Authors using an earthquake source usually located the thrust at the

40-km Fault (e.g. Matsuyama et al., 2000), although movement along this fault was clearly dip-slip to the north, with the only active fault segment to the west of the Amphitheatre. Other combinations of faulting, such as a steeply dipping fault and/or a splay fault off a blind thrust, are not supported by the marine data (e.g. Satake et al., 2003; Imamura and Hashi, 2003). These interpretations are not only in conflict with the evidence from the marine data but, as alternative tsunami sources, they do not reproduce the arrival time of the tsunami from the earthquake. Alternative slumps (e.g. Satake et al., 2003) located on the Upraised Block are too small to source the measured tsunami and would not produce a LDN wave on the PNG coast. To fully utilise the marine data set (comprising bathymetry, seismic, images, and samples) one needs interpretations and integration in their entirety. The bathymetry and sampling evidence from the Amphitheatre indicate a submarine slump of recent origin located near the centre of the Amphitheatre. Each individual feature observed in isolation might well be attributed to another cause, such as an earthquake (e.g. Matsuyama et al., 1999; Satake et al., 2003). However, it is the use of all the marine data that demonstrates the slump as the most likely tsunami source.

With regard to the timing of tsunami impact on the shore, this is normally identified from tide gauge data. Without tide gauge data, the quantitative approach of seismologists could not be followed, and in this context the evidence from survivors on the delay between main shock and tsunami strike was discounted (e.g. Geist, 2000). There is no doubt that contradictory reporting of tsunami arrival times contributed to survivor's evidence being ignored. There are good reasons why the reports varied. 1) The survivors would have been traumatised, and their reporting confused. 2) Felt effects of the earthquake would have varied along the coast because of changes in composition of the substrate. On the sand spit, earthquake energy would have been absorbed and dissipated, and here we know of significant fluid expulsion and sediment liquefaction (McSaveny et al., 2000). Farther east, at Malol and Aitape, the presence of hard limestone resulted in far greater felt effects. 3) There is also evidence that at some locations (such as Malol) the tsunami may have struck at the same time as the aftershocks. 4) There are significant variations in tsunami attack along the shoreline found from modelling results. However, not all of the reports were 'relative' and timed according to the earthquake or the aftershocks. In the east, at Aitape, accurate reporting on the tsunami arrival time was based on watches, clocks, and radios that give an absolute time (Davies, 1999). These showed the tsunami arriving there 5 min after the aftershocks and approximately 25 min after the main shock. This evidence is as accurate as the timing from most tide gauge records.

7 Conclusions

The PNG tsunami has resulted in the development of new and improved models of tsunami generation that more realistically represent SMF tsunami sources. Additionally, it has stimulated the development of propagation and runup models that may be applied to all tsunami sources. Although controversial, the event has resulted in a global re-evaluation of the tsunami hazard from SMFs and of anomalous tsunami events, where earthquake magnitude does not correlate with measured runup. Since 1999, the west coast of the USA has received a great deal more focussed attention on SMF tsunami hazard (e.g. Eichhubl et al., 2002; Lee et al., 2003, 2004; Bohannon and Gardner, 2004; Locat et al., 2004; Normark et al., 2004; Greene et al., 2005). One of the largest marine survey programmes ever carried out over a SMF has been off Norway to investigate the potential hazard from a future failure in the area of the Storegga Landslide, although the motivation for the research was mainly to do with the safe extraction of gas from the underlying Ormen Lange Gasfield (e.g. Bondevik et al., 2005; Løvholt et al., 2005; Solheim et al., 2005). The Storegga Landslide, dated at 8200 years BP, resulted in a tsunami with significant runup along the NW European coastline.

Although several recent tsunamis (e.g. Grand Banks, 1929; Seward, 1964) were known to be sourced by SMFs, and these events indicated their potential hazard, the PNG tsunami was largely unexpected. It was a "wake-up" call with regard to the tsunami hazard from SMFs triggered by modest size earthquakes. The initial motivation for the research on the PNG tsunami was undoubtedly due to the scale of the catastrophe that resulted in the funding, at very short notice, of costly marine scientific investigations into the cause of the disaster.

The controversy over the source of the PNG tsunami, now accepted by most scientists as a submarine slump, was mainly because SMFs were not considered a source of catastrophic tsunamis before 1998. In addition, the modelling of SMF tsunami sources was almost exclusively confined to tsunami generation by thin, translational landslides or sediment flows. As a consequence, there were no validated models for SMFs formed of thick, cohesive, rotational slumps. Early consideration of the cause of the tsunami tended to discount qualitative evidence, such as that from survivors. All these factors contributed to the mistaken identification by many scientists of an earthquake source for the tsunami.

The marine surveys carried out in 1999 were the first organised specifically to identify the offshore cause of a recent tsunami. They have led to marine geologists becoming more actively involved in tsunami research, thereby providing a new approach to researching tsunami hazards. The application of swath bathymetry (a recent technological development in marine science) together with other more traditional technologies used in marine surveying, such as sub-bottom seismic, seabed photography, and sediment coring, provide

data essential to the identification of SMFs. However, to maximise their effectiveness, the marine data acquired have to be fully integrated, thereby providing a powerful tool for tsunami hazard assessment. Marine data is a requisite for SMF modelling. It also informs on the background geology and the dating of events. Although laboratory based studies underpin our understanding of tsunami generation from SMFs, field examples are essential in validating theoretical analyses and numerical models.

Since 1998, modelling of SMF tsunamis has advanced to the stage where integrated models, based on SMF architecture, can account for the complete tsunami process from tsunami source through wave generation and propagation to tsunami runup and inundation, similar to co-seismic tsunamis. The direct result of PNG is our increased awareness of how SMFs cause tsunamis in both the near and far field. They are not dipoles (as earthquakes are), they cannot be modelled using a constant velocity, their maximum velocity scales with SMF size, and wave amplitude decay in the far field is an order of magnitude less than previously supposed. A lot has been learned over the last decade.

It should be cautioned however, that current SMF tsunami source models still require many simplifications and assumptions, and that more work is needed to refine existing models of failure from all types of SMF (e.g. Greene et al., 2005; Waythomas et al., 2006). In 1998, there was little appreciation of the importance of centre of mass motion on tsunami generation. For the same size and density SMF, tsunami amplitudes and wavelengths can differ by up to a factor of five depending on the centre of mass motion (Grilli and Watts, 2005). The most important measure of centre of mass motion is the SMF initial acceleration.

At present, PNG remains the only tsunami clearly identified as caused by a submarine slump. It is a benchmark case. By contrast with translational landslides, SMF tsunamis caused by slumps are still a largely unknown hazard for coastal communities. Notwithstanding, the methodologies developed to study the PNG event now provide the basis for assessing other vulnerable areas.

Acknowledgements. This paper was funded in part by the US National Science Foundation through grant CMS-0100223 made to S. Grilli. Funding was also provided by Applied Fluids Engineering, Inc. and the British Geological Survey. We thank A. Simpson, the Director of the Pacific Applied Geosciences Commission (SOPAC) for his foresight in stimulating the JAMSTEC/SOPAC surveys, JAMSTEC for their organisation and provision of the ships and personnel, and the Government of Japan for funding the surveys. Our shipboard colleagues on the marine expeditions are acknowledged for their many conversations regarding the source of the PNG tsunami. Thanks go to D. Mosher and an anonymous reviewer for reading and commenting on the original manuscript draft that resulted in significant improvements. D. Tappin publishes with the permission of the Executive Director, British Geological Survey, (NERC) United Kingdom. Mention of trade names is for identification purposes only and does not constitute endorsement.

Edited by: S. Tinti
Reviewed by: D. Mosher and another anonymous referee

References

Abe, K.: Size of great earthquakes of 1837–1974 inferred from tsunami data, J. Geophys. Res., 84, 1561–1568, 1979.

Ammon, C. J., Kanimori, H., Lay, T., and Velasc, A. A.: The 17 July 2006 Java tsunami earthquake, Geophys. Res. Lett., 33, L24308, doi:10.1029/2006GL028005, 2006.

Bardet, J.-P., Synolakis, C. E., Davies, H. L., Imamura, F., and Okal, E. A.: Landslide tsunamis: Recent findings and research directions, Pure Appl. Geophys., 160(2003) 1793–1809, doi:10.1007/s00024-003-2406-0, 2003.

Bohannon, R. G. and Gardner, J. V.: Submarine landslides of San Pedro Escarpment, southwest of Long Beach, California, Mar. Geol., 203, 261–268, 2004.

Bondevik, S., Løvholt, A., Harbitz, C. B., Mangerud, J., Dawson, A., and Svendsen, J. I.: The Storegga Slide tsunami – comparing field observations with numerical simulations, Mar. Petroleum Geology, 22, 195–208, 2005.

Borrero, J. C.: Changing field data gives better model results; an example from Papua New Guinea, Proc. Int. Tsunami Symp., 397–405, 2001.

Chen, Q., Kirby, J. T., Dalrymple, R. A., Kennedy, A. B., and Chawla, A.: Boussinesq study of wave transformation, breaking, and runup. II: 2-D, J. Wtrwy, Port, Coast, and Oc. Engrg., ASCE, 126, 1, 48–56, 2000.

Davies, H. L.: The Sissano tsunami 1998, University of Papua New Guinea Press, Port Moresby, Papua New Guinea, 1998.

Davies, H. L., Davies, J. M., Perembo, R. C. B., and Lus, W. Y.: The Aitape 1998 tsunami: Reconstructing the event from interviews and field mapping, edited by: Bardet, J.-P., Synolakis, C., and Okal, E. A., Pure Appl. Geophys., 160(2003) 1895–1922, doi:10.1007/s00024-003-2413-1, 2003.

Day, S. J., Watts, P., Grilli, S. T., and Kirby, J. T.: Mechanical models of the 1975 Kalapana, Hawaii earthquake and tsunami, Mar. Geol., 215, 59–92, 2005.

Edwards, B. D., Lee, H. J., and Field, M. E.: Mudflow generated by retrogressive slope failure, Santa Barbara Basin, California Continental Borderland, J. Sed. Res., A65, 57–68, 1995.

Eichhubl, P., Greene, H. G., and Maher, N.: Physiography of an active transpressive margin basin; high-resolution bathymetry of the Santa Barbara Basin, southern California continental borderland, Mar. Geol., 184, 95–120, 2002.

Enet, F., Grilli, S. T., and Watts, P.: Laboratory experiments for tsunamis generated by underwater landslides: Comparison with numerical modeling, Proc. 13th Int. Offshore and Polar Engineering Conference, ISOPE03, Honolulu, Hawaii, 3, 372–379, 2003.

Enet, F. and Grilli, S. T.: Tsunami landslide generation: Modelling and experiments, in: Proc. 5th Intl. on Ocean Wave Measurement and Analysis (WAVES 2005, Madrid, Spain, July 2005), ASCE Publication, paper 88, 10 pp, 2005.

Enet, F. and Grilli, S. T.: Experimental study of tsunami generation by three-dimensional rigid underwater landslides, J. Wtrwy, Port, Coast, and Oc. Engrg., 133(6), 442–454, 2007.

Fryer, G. J., Watts, P., and Pratson, L. F.: Source of the great tsunami of 1 April 1946: a landslide in the upper Aleutian forearc, Mar. Geol., 203, 201–218, 2004.

Geist, E. L.: Source characteristics of the July 17, 1998 Papua New Guinea Tsunami, (abs.), Eos Trans. Am. Geophys. Union, 79, Fall Meeting. Suppl. F571-2, 1998a.

Geist, E. L.: Local tsunamis and earthquake source parameters, Adv. Geophys., 39, 117–209, 1998b.

Geist, E. L.: Origin of the 17 July, 1998 Papua New Guinea tsunami: Earthquake or landslide?, Seis. Res. Lett., 71, 344–351, 2000.

Geist, E. L.: Reply to comment by E. A. Okal and C. E. Synolakis on "Origin of the 17 July 1998 Papua New Guinea tsunami: Earthquake or landslide?" by E. L. Geist, Seis. Res. Lett., 72(3), 367–389, 2001.

Gelfenbaum, G. and Jaffe, B. E.: Erosion and sedimentation of the Papua New Guinea tsunami, edited by: Bardet, J.-P., Synolakis, C., and Okal, E. A., Pure Appl. Geophys., 160(2003), 1969–1999, doi:10.1007/s00024-003-2416-y, 2003.

Greene, H. G., Murai, L. Y., Watts, P., Maher, N. A., Fisher, M. A., Paull, C. E., and Eichhubl, P.: Submarine landslides of the Santa Barbara Basin: Potential tsunami generators, Nat. Hazards Earth Syst. Sci., 6, 63–88, 2005, http://www.nat-hazards-earth-syst-sci.net/6/63/2005/.

Grilli, S. T., Ioualalen, M., Asavanant, J., Shi, F., Kirby, J., and Watts, P.: Source constraints and model simulation of the December 26, 2004 Indian Ocean tsunami, J. Waterway Port Coastal and Ocean Engineering, 133(6), 414–428, 2007.

Grilli, S. T. and Watts, P.: Modelling of waves generated by a moving submerged body: Applications to underwater landslides, Engrg. Analysis with Boundary Elements, 23(8), 645–656, 1999.

Grilli, S. T., Vogelmann, S., and Watts, P.: Development of a 3D numerical wave tank for modelling tsunami generation by underwater landslides, Engrg. Analysis with Boundary Elements, 26(4), 301–313, 2002.

Grilli, S. T. and Watts, P.: Tsunami generation by submarine mass failure part I: Modeling, experimental validation, and sensitivity analyses, J. Wtrwy, Port, Coast, and Oc. Engrg., ASCE, 131(6), 283–297, 2005.

Gutenberg, B.: Tsunamis and earthquakes, B. Seismol. Soc. Am., 29, 517–526, 1939.

Hammack, J. L.: A note on tsunamis: Their generation and propagation in an ocean of uniform depth, J. Fluid Mech., 60, 769–799, 1973.

Hampton, M.: The role of subaqueous debris flow in generating turbidity currents, J. Sed. Petrol., 42, 775–993, 1972.

Hampton, M. A., Lee, H. J., and Locat, J.: Submarine landslides, Rev. Geophys., 34(1), 33–59, 1996.

Heezen, B. C. and Ewing, M.: Turbidity currents and submarine slumps, and the 1929 Grand Banks Earthquake, Am. J. Sci., 250, 849–873, 1952.

Heezen, B. C., Ericsson, D. B., and Ewing, M.: Further evidence of a turbidity current following the 1929 Grand Banks earthquake, Deep Sea Res., 1, 193–202, 1954.

Hebenstreit, G. T. (Ed.): Tsunami research at the end of a critical decade, Adv. Nat. Technol. Res., Kluwer Academic Publishers, 282 pp, 2001.

Heinrich, P.: Nonlinear water waves generated by submarine and aerial landslides, J. Wtrwy, Port, Coast, and Oc. Engrg., ASCE, 118(3), 249–266, 1992.

Heinrich, P., Piatanesi, A., Hébert, H., and Okal, E. A.: Near-field modelling of the July 17, 1998 event in Papua New Guinea, Geophys. Res. Lett., 27, 3037–3040, 2000.

Hurakawa, N.: A fault plane of the 1998 Papua New Guinea earthquake estimated from relocated aftershocks using data of the International Data Center of CTBT, Zisin, 52, 95–99, 1998 (in Japanese).

Imamura, F. and Goto, C.: Truncation error in numerical tsunami simulation by the finite difference method, Coastal Engrg. Japan, 31(2), 245–263, 1998.

Imamura, F., Gica, E., Takahashi, T., and Shuto, N.: Numerical simulation of the 1992 Flores tsunami: Interpretation of tsunami phenomena in northeastern Flores Island and damage at Babi Island, Pure Appl. Geophys., 144, 555–568, 1995.

Imamura, F. and Gica, E. C.: Numerical model for tsunami generation due to subaqueous landslide along a coast, Sci. Tsunami Hazards, 14, 13–28, 1996.

Imamura, F. and Hashi, K.: Re-examination of the tsunami source of the 1998 PNG earthquake tsunami, Eos, Trans. Am. Geophys. Union, (abstract), 81, 143, 2000.

Imamura, F., Hashi, K., and Imteaz, M. A.: Modelling for tsunamis generated by landsliding and debris flow, in: Tsunami research at the end of a critical decade, edited by: Hebenstreit, G., Kluwer Academic Publishers, Dordrecht, 209–228, 2001.

Imamura, F. and Hashi, K.: Re-examination of the source mechanism of the 1998 Papua New Guinea earthquake and tsunami, Pure Appl. Geophys., 160(2003), 2071–2086, doi:10.1007/s00024-003-2420-2, 2003.

Imran, J., Parker, G., Locat, J., and Lee, H.: 1D numerical model of muddy subaqueous and subaerial debris flow, J. Hyd. Eng., ASCE, 127(11), 959–968, 2001.

Ioualalen, M., Pelletier, B., Regnier, M., and Watts, P.: Numerical modeling of the 26th November 1999 Vanuatu tsunami, J. Geophys. Res., 111, C06030, doi:10.1029/2005JC003249, 2006.

Ioualalen, M., Asavanant, J., Kaewbanjak, N., Grilli, S. T., Kirby, J. T., and Watts, P.: Modeling the 26th December 2004 Indian Ocean tsunami: Case study of impact in Thailand, J. Geophys. Res., 112, C07024, doi:10.1029/2006JC003850, 2007.

Iwasaki, S.: The wave forms and directivity of a tsunami generated by an earthquake and a landslide, Sci. Tsunami Hazards, 15, 23–40, 1997.

Iwasaki, S. and Satake, K.: Numerical study of the source of the July 1998 Papua New Guinea tsunami, in: Tsunami research at the end of a critical decade, edited by: Hebenstreit, G., Kluwer Academic Publishers, Dordrecht, 2001.

Jaffe, B. E. and Gelfenbaum, G.: Using tsunami deposits to improve assessment of tsunami risk, Solutions to Coastal Disasters '02 Conference Proceedings, 836–847, 2000.

Jiang, L. and LeBlond, P. H.: The coupling of a submarine slide and the surface wave which it generates, J. Geophys. Res., 97, 12 731–12 744, 1992.

Jiang, L. and LeBlond, P. H.: Three dimensional modelling of tsunami generation due to submarine mudslide, J. Phys. Ocean., 24, 559–573, 1994.

Johnson, J. M. and Satake, K.: Estimation of seismic moment and slip distribution of the April 1, 1946 Aleutian tsunami earthquake, J. Geophys. Res., 102, 11 765–11 774, 1997.

Kanoglu, U. and Synolakis, C. E.: Long wave runup on piecewise

linear topographies, J. Fluid Mech., 374, 1–28, 1998.
Kanamori, H.: Mechanisms of tsunami earthquakes, Phys. Earth Planet. Inter., 6, 346–359, 1972.
Kawata, Y., Benson, B. C., Borrero, J. L., Davies, H. L., de Lange, W. P., Imamura, F., Letz, H., Nott, J., and Synolakis, C. E.: Tsunami in Papua New Guinea was as intense as first thought, Eos, Trans. Amer. Geophys. Union, 80(9), 101, 104–105, 1999.
Keating, B. H. and McGuire, W. J.: Island edifice failures and associated tsunami hazards, Pure Appl. Geophys., 157, 899–955, 2000.
Kennedy, A. B., Chen, Q., Kirby, J. T., and Dalrymple, R. A.: Boussinesq modelling of wave transformation, breaking, and runup. I: 1D, J. Wtrwy, Port, Coast, and Oc. Engrg., ASCE, 126(1), 39–47, 2000.
Kikuchi, M., Yamanaka, Y., Abe, K., and Morita, Y.: Source rupture process of the Papua New Guinea earthquake of July 17th, 1998 inferred from teleseismic body waves, Earth Planets Space, 51, 1319–1324, 1999.
LeBlond, P. H. and Jones, A.: Underwater landslides ineffective at tsunami generation, Sci. Tsunami Hazards, 13, 25–26, 1995.
Lee, H. J., Kayen, R. E., Gardner, J. V., and Locat, J.: Characteristics of several tsunamigenic submarine landslides, in: Submarine Mass Movements and their Consequences, edited by: Locat, J. and Mienert, J., Kluwer, The Netherlands, 357–366, 2003.
Lee, H. J., Normark, W. R., Fisher, M. A., Greene, H. G., Edwards, B. D., and Locat, J.: Timing and extent of submarine landslides in Southern California, Proceedings, Offshore Technology Conference, Houston TX, OTC Paper 16744, 2004.
Lee, H. J.: Undersea landslides: Extent and significance in the Pacific Ocean, an update, Nat. Hazards Earth Syst. Sci., 5, 877–892, 2005,
http://www.nat-hazards-earth-syst-sci.net/5/877/2005/.
Liu, P. L.-F., Yeh, H., Lin, P., Chang, K.-T., and Cho, Y.-S.: Generation and evolution of edge-wave packets, Phys. Fluids, 10(7), 1635–1657, 1998.
Locat, J., Lee, H. J., Locat, P., and Imran, J.: Numerical analysis of the mobility of the Palos Verdes debris avalanche, California, and its implication for the generation of tsunamis, Mar. Geol., 203, 269–280, 2004.
López, A. M. and Okal, E. A.: A seismological reassessment of the source of the 1946 Aleutian "tsunami" earthquake, Geophys. J. Intl., 165, 835–849, 2006.
Løvholt, F., Harbitz, C. B., and Haugen, K. B.: A parametric study of tsunamis generated by submarine slides in the Ormen Lange/Storegga area off western Norway Marine and Petroleum, Geology, 22, 219–231, 2005.
Lynett, P. J., Borrero, J. C., Liu, P. L-F., and Synolakis, C. E.: Field survey and numerical simulations: A review of the 1998 Papua New Guinea tsunami, Pure Appl. Geophys., 160, 2119–2146, doi:10.1007/s00024-003-2422-0, 2003.
Matsumoto, T., Tappin, D. R., and SOS Shipboard Party: NT99-02 Cruise Report – Papua New Guinea, JAMSTEC, 102 pp, 1999.
Matsumoto, T., Tappin, D. R., and SOS Shipboard Party.: Possible coseismic large-scale landslide off the northern coast of Papua New Guinea in July 1998: Geophysical and geological results from the SOS cruises, edited by: Bardet, J,-P,, Synolakis, C.m and Okal, E. A., Pure Appl. Geophys., 160(2003), 1923–1943, doi:10.1007/s00024-003-2414-0, 2003.
Matsuyama, M., Walsh, J. P., and Yeh, H.: The effect of bathymetry on tsunami characteristics at Sissano Lagoon, Papua New Guinea, Geophys. Res. Lett., 26, 3513–3516, 1999.
McCue, K. F.: An AGSO perspective of PNG's tsunamagenic earthquake of 17 July 1998, AusGeo Int., 9, 1998.
McMurtry, G. M., Fryer, G. J., Tappin, D. R., Wilkinson, I. P., Williams, M., Fietzke, J., Garbe-Schoenberg, D., and Watts, P.: Megatsunami deposits on Kohala Volcano, Hawaii from flank collapse of Mauna Loa, Geology, 32(9), 741–744, 2004.
McSaveny, M. J., Goff, J. R., Darby, D. J., Goldsmith, P., Barnett, A., Elliot, S., and Nongkas, M.: The 17 July, 1998 tsunami, Papua New Guinea: Evidence and initial interpretation, Mar. Geol., 170, 81–92, 2000.
Milne, J.: Earthquakes and other earth movements, Paul, Trench, Trübner & Co., London, U.K., 1898.
Montessus de Ballore, F.: La science séismologique, Colin, Paris, France, 1907.
Murty, T. S.: Submarine slide-generated water waves in Kitimat Inlet, British Columbia, J. Geophys. Res., 84(C12), 7777–7779, 1979.
Newman, A. V. and Okal, E. A.: Moderately slow character of the July 17, 1998 Sandaun earthquake as studied by teleseismic energy estimates, (abs.), Eos Transactions, American Geophysical Union, 79, Fall Meeting, Supplement F564, 1998a.
Newman, A. V. and Okal, E. A.: Teleseismic estimates of radiated seismic energy: The $E/M0$ discriminant for tsunami earthquakes, J. Geophys. Res., 103, 26 885–26 898, 1998b.
Normark, W. R., McGann, M., and Sliter, R.: Age of Palos Verdes submarine debris avalanche, southern California, Mar. Geol., 203, 247–260, 2004.
O'Grady, D. B., Syvitski, J. P. M., Pratson, L. F., and Sarg, J. F.: Categorizing the morphologic variability of siliciclastic passive continental margins, Geology, 28(3), 207–210, 2000.
Okal, E. A.: The probable source of the 1998 Papua New Guinea tsunami as expressed in oceanic T waves, Eos, Trans. Amer. Geophys. Un., 80(46), F750, 1999.
Okal, E. A.: T waves from the 1998 Sandaun PNG sequence: Definitive timing of the slump, Eos, Trans. Am. Geophys. Union, (abstract), 81(48), 142, 2000.
Okal, E. A. and Synolakis, C. E.: Comment on "Origin of the 17 July 1998 Papua New Guinea tsunami: Earthquake or landslide?" by E. L. Geist, Seis. Res. Lett., 72(3), 363–366, 2001.
Okal, E. A. and Synokalis C. E.: A Theoretical Comparison of Tsunamis from Dislocations and Landslides, Pure Appl. Geophys., 160, 2177–2188, doi:10.1007/s00024-003-2425-x, 2003.
Piper, D. J. W. and McCAll, C.: A synthesis of the distribution of submarine mass movements on the eastern Canadian Margin, in: Submarine mass movements and their consequences, edited by: Locat, J. and Mienert, J., Kluwer Academic Publishers, 291–298, 2003.
Prior, D. B. and Coleman, J. M.: Submarine landslides: Geometry and nomenclature, Z. Geomorph. N. F., 23(4), 415–426, 1979.
Satake, K. and Tanioka, Y.: The July 1998 Papua New Guinea earthquake and tsunami: A generation model consistent with various observations, Eos, Trans. Am. Geophys. Union, 80, 750, 1999.
Satake, K. and Tanioka, Y.: The July 1998 Papua New Guinea earthquake: mechanism and quantification of unusual tsunami generation, Pure Appl. Geophys., 160(2003), 2087–2118, doi:10.1007/s00024-003-2421-1, 2003.
Schwab, W. C., Lee, H. J., and Twichell, D. C.: Submarine land-

slides: Selected studies in the U.S. exclusive economic zone, U.S. Geol. Surv. Bull. 2002, US, Dept. of Interior, Washington, D.C., 1993.

Simpson, D. W.: Triggered earthquakes, 14 Ann. Rev. Earth Planetary Sciences, 21, 1986.

Solheim, A., Bryn, P., Berg, K., and Mienert, J. (Eds): Ormen Lange – an integrated study for the safe development of a deep-water gas field within the Storegga Slide Complex, NE Atlantic continental margin, Mar. Petrol. Geol., 22, 1–318, 2005.

Sweet, S., Silver, E., Davies, H., Matsumoto, T., Watts, P., and Synolakis, C. E.: Seismic reflection images of the source region of the Papua New Guinea tsunami of July 17, 1998, Eos, Trans. Am. Geophys. Union, Fall Meeting Suppl., Abstract S51C-02, 1999.

Sweet, S. and Silver, E. A.: Tectonics and slumping in the source region of the 1998 Papua New Guinea tsunami from seismic reflection images, Pure Appl. Geophys., 160(2003), 1945–1968, doi:10.1007/s00024-003-2415-z, 2003.

Synolakis, C. E., Bardet, J. P., Borrero, J. C., Davies, H. L., Okal, E. A., Silver, E. A., Sweet, S., and Tappin, D. R.: The slump origin of the 1998 Papua New Guinea tsunami, Proc. Royal. Soc., London, 458(2020), 763–790, 2002.

Takahashi, T. and Kawata, Y.: Energy concentration and recurrence of the 1998 Papua New Guinea tsunami, Eos Transactions, American Geophysical Union, 79, Fall Meeting, Supplement, F572, 1998.

Tanioka, Y.: Analysis of the far-field tsunami generated by the 1998 PNG earthquake, Geophys. Res. Lett., 22, 3393–3396, 1999.

Tappin, D. R., Matsumoto, T., Watts, P., Satake, K., McMurtry, G. M., Matsuyama, M., Lafoy, Y., Tsuji, Y., Kanamatsu, T., Lus, W., Iwabuchi, Y., Yeh, H., Matsumotu, Y., Nakamura, M., Mahoi, M., Hill, P., Crook, K., Anton, L., and Walsh, J. P.: Sediment slump likely caused 1998 Papua New Guinea Tsunami, EOS, Transactions of the American Geophysical Union, 80, p. 329, 334, 340, 1999.

Tappin, D. R., Watts, P., McMurtry, G. M., Lafoy, Y., and Matsumoto, T.: The Sissano, Papua New Guinea tsunami of July 1998 – Offshore evidence on the source mechanism, Mar. Geol., 175, 1–23, 2001.

Tappin, D. R., Watts, P., McMurtry, G. M., Lafoy, Y., and Matsumoto, T.: Prediction of slump generated tsunamis: The July 17th 1998 Papua New Guinea event, Sci. Tsunami Hazards, 20(4), 222–238, 2002.

Tappin, D. R., Watts, P., and Matsumoto, T.: Architecture and failure mechanism of the offshore slump responsible for the 1998 PNG tsunami, in: Submarine mass movements and their consequences, edited by: Locat, J. and Meinert, J., Kluwer Academic Publishers, pp. 383–392, 2003.

Tappin, D. R. (Ed): Special Issue; submarine slump generated tsunamis, Mar. Geol., 203(3–4), 199–380, 2004.

Terzaghi, K.: Varieties of submarine slope failures: 8th Tex. Conf. of Soil Mech. and Found. Eng., Proc., Special Publication 29, Bureau Eng. Research, Tex. University, p. 1–41, 1956.

Tinti, S., Bortolucci, E., and Chiavettieri, C.: Tsunami excitation by submarine slides in shallow-water approximation, Pure Appl. Geophys., 158, 759–797, 2001.

Titov, V. and Gonzalez, F.: Numerical study of the source of the July 1998 PNG earthquake (abs.), Eos Transactions. Am. Geophys. Union, 79, Fall Meeting, Supplement, F564, 1998.

Titov, V. and Synolakis, C. E.: Numerical modelling of tidal wave runup, J. Wtrwy., Port, Coast, and Oc. Engnrg., 124, 157–171, 1998.

Turner, A. K. and Schuster, R. L.: Landslides: Investigation and mitigation. Special Report 247, Trans. Res. Board, National Academy Press, Washington, D.C., 1996.

von Huene, R, Ranero, C. R., and Watts, P.: Tsunamigenic slope failure along the Middle America Trench in two tectonic settings, Mar. Geol., 203, 303–317, 2004.

Ward, S. N.: Landslide tsunami, J. Geophys. Res., 106(6), 11 201–11 215, 2001.

Watts, P.: Water waves generated by underwater landslides, PhD thesis, California Inst. of Technol., Pasadena, CA., 1997.

Watts, P.: Wavemaker curves for tsunamis generated by underwater landslides, J. Wtrwy, Port, Coast, and Oc. Engrg., ASCE, 124(3), 127–137, 1998.

Watts, P., Borrero, J. C., Tappin, D. R., Bardet, J.-P., Grilli, S. T., and Synolakis, C. E.: Novel simulation technique employed on the 1998 Papua New Guinea tsunami, in: Proceedings of 22nd General Assembly IUGG, Birmingham, UK JSS42, Abstract, 1999.

Watts, P.: Tsunami features of solid block underwater landslides, J. Wtrwy, Port, Coast, and Oc. Engrg., ASCE, 126(3), 144–152, 2000.

Watts, P., Imamura, F., and Grilli, S. T.: Comparing model simulations of three benchmark tsunami generation cases, Sci. Tsunami Hazards, 18(2), 107–124, 2000.

Watts, P.: Some opportunities of the landslide tsunami hypothesis, Sci. Tsunami Hazards, 19(3), 126–149, 2001.

Watts, P.: The need for underwater landslide hazards prediction, Sci. Tsunami Hazards, 20(2), 95–101, 2002.

Watts, P.: Probabilistic predictions of landslide tsunamis off Southern California, Mar. Geol., 203, 281–301, 2004.

Watts, P. and Grilli, S. T.: Underwater landslide shape, motion, deformation, and tsunami generation. Proceedings of the 13th International Offshore and Polar Engineering Conference, ISOPE03, Honolulu, Hawaii, 3, 364–371, 2003.

Watts, P., Grilli, S. T., Kirby, J. T., Fryer, G. J., and Tappin, D. R.: Landslide tsunami case studies using a Boussinesq model and a fully nonlinear tsunami generation model, Nat. Hazards Earth Syst. Sci., 3, 391–402, 2003, http://www.nat-hazards-earth-syst-sci.net/3/391/2003/.

Watts, P., Grilli, S. T., Tappin, D. R., and Fryer, G. J.: Tsunami generation by submarine mass failure part II: Predictive equations and case studies, J. Wtrwy, Port, Coast, and Oc. Engrg., ASCE, 131(6), 298–310, 2005a.

Watts, P., Ioualalen, M., Grilli, S. T., Kirby, J. T., and Shi, F.: Numerical simulation of the December 26, 2004 Indian Ocean tsunami using a higher-order Boussinesq model, Proc. 5th Intl. Symp. on Ocean Wave Measurement and Analysis (Waves 2005, Madrid, Spain, July 2005), IAHR Publication, paper 221, 10 pp, 2005b.

Waythomas, C. F. and Watts, P.: Numerical Simulation of Tsunami Generation by Pyroclastic Flow at Aniakchak Volcano, Alaska, Geophys. Res. Lett., 30(14), 1751–1755, 2003.

Waythomas, C. F., Watts, P., and Walder, J. S.: Numerical simulation of tsunami generation by cold volcanic mass flows at Augustine Volcano, Alaska, Nat. Hazards Earth Syst. Sci., 6, 671–685, 2006, http://www.nat-hazards-earth-syst-sci.net/6/671/2006/.

Wei, G. and Kirby, J. T.: Time-dependent numerical code for extended Boussinesq equations, J. Wtrwy, Port, Coast, and Oc. Engrg., ASCE, 121(5), 251–261, 1995.

Wei, G., Kirby, J. T., Grilli, S. T., and Subramanya, R.: A fully nonlinear Boussinesq model for free surface waves. Part 1: Highly nonlinear unsteady waves, J. Fluid Mech., 294, 71–92, 1995.

Wiegel, R. L.: Laboratory studies of gravity waves generated by the movement of a submarine body, Trans. Am. Geophys. Union, 36(5), 759–774, 1955.